The 29 June 2000 Supercell Observed during STEPS. Part II: Lightning and Charge Structure

KYLE C. WIENS,* STEVEN A. RUTLEDGE, AND SARAH A. TESSENDORF

Department of Atmospheric Science, Colorado State University, Fort Collins, Colorado

(Manuscript received 25 June 2004, in final form 21 March 2005)

ABSTRACT

This second part of a two-part study examines the lightning and charge structure evolution of the 29 June 2000 tornadic supercell observed during the Severe Thunderstorm Electrification and Precipitation Study (STEPS). Data from the National Lightning Detection Network and the New Mexico Tech Lightning Mapping Array (LMA) are used to quantify the total and cloud-to-ground (CG) flash rates. Additionally, the LMA data are used to infer gross charge structure and to determine the origin locations and charge regions involved in the CG flashes. The total flash rate reached nearly 300 min^{-1} and was well correlated with radar-inferred updraft and graupel echo volumes. Intracloud flashes accounted for 95%–100% of the total lightning activity during any given minute. Nearly 90% of the CG flashes delivered a positive charge to ground (+CGs). The charge structure during the first 20 min of this storm consisted of a midlevel negative charge overlying lower positive charge with no evidence of an upper positive charge. The charge structure in the later (severe) phase was more complex but maintained what could be roughly described as an inverted tripole, dominated by a deep midlevel (5–9 km MSL) region of positive charge. The storm produced only two CG flashes (both positive) in the first 2 h of lightning activity, both of which occurred during a brief surge in updraft and hail production. Frequent +CG flashes began nearly coincident with dramatic increases in storm updraft, hail production, total flash rate, and the formation of an F1 tornado. The +CG flashes tended to cluster in or just downwind of the heaviest precipitation, which usually contained hail. The +CG flashes all originated between 5 and 9 km MSL, centered at 6.8 km (−10°C), and tapped LMA-inferred positive charge both in the precipitation core and (more often) in weaker reflectivity extending downwind. All but one of the −CG flashes originated from >9 km MSL and tended to strike near the precipitation core.

1. Introduction

The majority of cloud-to-ground (CG) lightning flashes produced by warm-season thunderstorms lower negative charge to ground (−CG). However, some severe thunderstorms often produce copious positive cloud-to-ground (+CG) flashes with little, if any −CG lightning activity (MacGorman and Burgess 1994; Stolzenburg 1994; Carey and Rutledge 1998; Lang and Rutledge 2002). In addition, +CG-dominated severe storms are frequent within a corridor extending northward from the Colorado–Kansas border into Canada (Orville and Huffines 2001; Zajac and Rutledge 2001; Carey et al. 2003b). The Severe Thunderstorm Electrification and Precipitation Study (STEPS; Lang et al. 2004a) was conducted in this +CG corridor during the summer of 2000. One of the primary goals of STEPS is to understand why the severe storms in this region are often dominated by +CG lightning. In pursuit of this goal, Tessendorf et al. (2005, hereafter Part I) used Doppler–polarimetric radar along with a particle growth model to investigate the kinematic and microphysical evolution of a +CG-dominated supercell storm that occurred on 29 June 2000 in northwestern Kansas. Herein, in Part II, we concentrate on the evolution of this storm's lightning activity and diagnosed charge structure.

As reviewed in Williams (1989, 2001), thunderstorms commonly have a tripole charge structure consisting of a dominant negative charge region between −10° and

* Current affiliation: Space and Remote Sensing Group, Los Alamos National Laboratory, Los Alamos, New Mexico.

Corresponding author address: Kyle C. Wiens, Space and Remote Sensing Group, Los Alamos National Laboratory, ISR-2, Los Alamos, NM 87545.
E-mail: kwiens@lanl.gov

© 2005 American Meteorological Society

−25°C, a positive charge region above the negative, and an additional (usually small) positive charge near the 0°C level. The negative charge is termed dominant because it typically dominates the electric field measured at the ground and is the source region of the predominantly negative polarity CG flashes produced by warm-season thunderstorms (e.g., Krehbiel et al. 1979). Intracloud (IC) lightning flashes typically occur between the dominant negative and upper positive charge regions. The noninductive ice–ice collision (NIC) mechanism is thought to be primarily responsible for the formation of this charge structure (e.g., Takahashi 1978; Saunders and Peck 1998; Berdeklis and List 2001). Although the results from these and other cited studies differ to some degree, they consistently show that the polarity and amount of the charge transferred is dependent on temperature, supercooled liquid water content, and impact velocity (or, equivalently, on temperature and riming rate). For a representative effective liquid water content of 1 g m^{-3}, the rimer gains negative charge at temperatures colder than about −10°C and gains positive charge at warmer temperatures and/or greater effective liquid water content. The temperature or height where the rimer charge switches from negative to positive has often been termed a charge reversal level. Following gravitational sedimentation and associated size sorting of the hydrometeors, the NIC mechanism may produce the dominant tripole structure commonly observed in thunderstorms.

There are deviations, however, from this basic tripole structure. For example, Stolzenburg et al. (1998a,b,c) analyzed a large set of balloon-borne electric field soundings through thunderstorms. The updraft region of most of these storms consisted of the tripole structure with an additional negative charge region at the top, likely a screening layer. The heights of all the tripole charge regions were well-correlated with the strength of the updraft, with stronger updrafts associated with more elevated charge structures. The charge structures in the nonupdraft regions of these storms were consistently more complex and variable, with additional alternating charge regions below the lower positive. The magnitude of the electric field was also consistently greater in the nonupdraft regions. Stolzenburg et al. (1998c) suggest that the NIC mechanism could explain the tripole structure in the updraft, but that additional processes (e.g., inductive charging, deposition of charge by lightning, screening layer production) might be more important in the strong electric field of the nonupdraft regions and could contribute to the more complex charge structure observed there.

Several recent studies have documented intriguing relationships between the polarity of CG lightning and thunderstorm severity. For example, in their investigation of 15 severe storms, MacGorman and Burgess (1994) found that storms with frequent +CG flashes often produced large hail during times when +CG flashes dominated the ground flash activity. Furthermore, if the dominant polarity of CG flashes switched to negative in these storms, the frequency of large hail reports and diameter of the reported hail usually decreased. In a survey of severe +CG-dominated storms, Stolzenburg (1994) also found that large hail was often reported in the vicinity of dense +CG flash activity. Carey and Rutledge (1998) found that when the 7 June 1995 supercell in northeast Colorado underwent a surge in overall growth and production of hail, the +CG and IC flash rates increased dramatically. However, most of the +CG strike locations were not within the hail region; rather, most of the +CG flashes struck ground downstream of the hail shaft beneath the downshear anvil region of the storm, and the +CG flash rate maximized after most of the hail had fallen out. In the case of the 30 May 1998 Spencer, South Dakota, tornadic storm, Carey et al. (2003a) found that the +CG flash rate and the percentage of +CG flashes increased dramatically during, or just after, pulses in storm growth. The most dramatic +CG flash rate increase occurred while the Spencer storm was producing its most intense (F4) tornado damage. The +CG flash rate decreased rapidly as the F4 damage ceased. The +CG flashes of the Spencer storm tended to cluster (in terms of strike location) near heavy precipitation cores while the −CG flashes tended to strike on the periphery. However, unlike the other studies summarized above, Carey et al. (2003a) noted that there was very little evidence of large hail (≥¾ in.) in the Spencer storm. Most of the precipitation from the Spencer storm consisted of heavy rain and small hail. Since the above studies included only ground strike data, they could not determine from where the +CG flashes originated.

As recently reviewed by Williams (2001), several hypotheses have been put forth to explain the charge structure leading to +CG flashes and +CG-dominated thunderstorms.

1) Tilted dipole (e.g., Brook et al. 1982; Curran and Rust 1992): A typical dipole or tripole charge structure is assumed. The shearing of the updraft by strong mid- to upper-level horizontal winds laterally displaces upper positive charge. This decreases the shielding effect of the main midlevel negative charge, thus exposing the upper positive charge to ground. The +CG flashes could then originate from this displaced upper positive charge.

2) Precipitation unshielding: A typical dipole or tripole charge structure is assumed. Much of the main negative charge is removed by descending precipitation during storm collapse, leaving the upper positive charge unshielded from the ground and more able to produce +CG flashes. Carey and Rutledge (1998) proposed this to explain the maximum +CG flash rates that trailed maximum hail rates by tens of minutes in the storm they studied.
3) Tripole with enhanced lower positive charge: Here, the lower positive charge of the "typical" tripole structure is enhanced and becomes a dominant charge region. As described by Williams (2001), this charge structure may occur due to extraordinarily broad, undiluted updrafts. This would allow for enhanced formation of hail, enhanced positive charging of larger hydrometeors by the NIC mechanism, and hence a larger reservoir of lower positive charge, which could lead to +CG domination of ground flashes. In addition, −CG flashes would be reduced because of the shielding effect of the enhanced lower positive charge and also because a broader, stronger updraft would further elevate the main negative charge region.
4) Inverted dipole or tripole: The charge structure is essentially reversed, with negative charge aloft and positive charge in the place of the usual main negative charge region. Analyses of lightning mapping (Krehbiel et al. 2000b; Zhang et al. 2001) and balloon-borne electric field soundings (Rust and MacGorman 2002; MacGorman et al. 2005; Rust et al. 2005) suggest that the thunderstorms in the STEPS region are sometimes inverted in polarity.

These hypotheses do not explicitly address an additional element of +CG lightning production, namely, a lower negative charge region. In a normal tripole configuration, the presence of the lower positive charge beneath the main negative charge is thought to locally enhance the electric field, which provides the impetus for the negative discharge to ground (e.g., Jacobson and Krider 1976). For the case of +CG flashes, a lower negative charge would provide a similar impetus for a main positive charge. Furthermore, Marshall and Stolzenburg (2002) used an idealized one-dimensional charge model to demonstrate that −CG (+CG) flashes are more energetically favorable if the lower positive (negative) charge is involved in the flash. In the more detailed modeling studies of Mansell (2000) and Mansell et al. (2002), CG flashes of either polarity did not occur without such a lower charge region.

Given the unique combination of coincident lightning mapping and Doppler–polarimetric radar observations of the storm of this study, we expect new insight into the electrification of severe storms dominated by +CG flashes. Specifically, this study addresses the following questions. 1) What was the charge structure of this storm and how did it evolve? 2) Where did the +CG flashes originate and what charge regions were involved in their production? 3) What were the kinematic and microphysical influences on the charge structure and lightning?

2. Data and methodology

The Colorado State University (CSU)–University of Chicago and Illinois State Water Survey (CHILL), National Center for Atmospheric Research S-band dual-polarization Doppler radar (S-Pol), and KGLD National Weather Service radar in Goodland, Kansas, comprised the triple-Doppler radar network. The three radars performed synchronized full volumetric scans of the storm every 5–7 min from 2130 UTC 29 June to 0015 UTC 30 June. All radar data were interpolated to a (0.5 km × 0.5 km × 0.5 km) Cartesian grid prior to analysis. Three-dimensional winds were obtained via synthesis of the multi-Doppler data for each volume scan. Data from the polarimetric radars (CSU–CHILL and S-Pol) were used to estimate the bulk hydrometeor type (e.g., rain, hail, graupel) within each grid box. Echo volumes of specific radar quantities were computed for the purpose of constructing time series of these quantities. These echo volumes were computed by simply counting up the number of Cartesian grid boxes that satisfied certain criteria (e.g., updraft >10 m s^{-1}, classified as hail, etc.), then multiplying this number by the volume (0.5 km)^3 of the grid box. See Part I for more detailed descriptions of the radar data and methodology.

The National Lightning Detection Network (NLDN; Cummins et al. 1998) provided measurements of the time, strike location, polarity, and peak current of CG flashes. According to Cummins et al., the NLDN detection efficiency is 80%–90% in the STEPS region. The NLDN data were used to calculate CG flash rates, to identify LMA sources associated with CG flashes, and to place the strike points of CG flashes within the context of the radar and LMA observations.

The New Mexico Tech Lightning Mapping Array (LMA; Rison et al. 1999; Krehbiel et al. 2000a) provided measurements of the time and three-dimensional location of very high frequency (VHF) radiation sources emitted by lightning discharges. For a given lightning flash, the LMA may locate hundreds to thousands of such VHF sources, resulting in detailed maps of the total lightning activity. Hamlin (2004) and Thom-

as et al. (2004) provide detailed descriptions of the LMA in general and of the LMA's use in the STEPS campaign in particular.

All times are referenced to universal time (UTC; local time = UTC − 6 h). All altitudes are referenced to mean sea level (MSL; ground level = 1.1 km MSL).

a. Charge structure determination

Analysis of LMA data on a flash-by-flash basis is an interpretative process guided by a realistic physical model of the lightning discharge. Recent interferometer measurements (Rhodes et al. 1994; Shao and Krehbiel 1996) and LMA measurements (Rison et al. 1999; Krehbiel et al. 2000a; Hamlin 2004; Thomas et al. 2004) support the bidirectional model that was originally proposed by Kasemir (1960) and recently advocated and described by Mazur and Ruhnke (1993). In this model, the lightning discharge initiates in the strong electric field between regions of net positive and negative charge. The discharge then propagates in opposite directions from the discharge origin with one direction advancing negative charge (called negative breakdown or negative leaders) and the other direction advancing positive charge (positive breakdown or positive leaders). The charge block experiments of Williams et al. (1985) and modeling studies of Mansell et al. (2002) provide circumstantial evidence that the discharges preferentially propagate into regions of higher charge density, with much denser branching in these regions.

Using this bidirectional model as a basis for physical interpretation, the temporal and spatial development of individual flashes were examined in a time-animated sense to infer the signs and locations of the charge regions involved in the flashes. As described in Rison et al. (1999), negative polarity breakdown is inherently noisier than positive polarity breakdown at the radio frequencies used by the LMA, resulting in far more LMA sources that map the negative breakdown than map the positive breakdown. Assuming that negative breakdown usually proceeds through positive charge regions, a given flash has a relatively greater number of LMA sources within (or indicative of) the positive charge region(s) involved in the flash. In addition, partial mapping of negative charge regions is possible when negative leaders retrace the path of the quieter positive leader. This retracing of the positive channel by negative breakdown seems to correspond to the recoil streamers described by Mazur and Ruhnke (1993). For a typical IC flash between two charge regions, the lightning mapping generally reveals a stratified bilevel structure. The relative number of LMA sources in each inferred charge region gives a rough idea of the charge structure; however, the spatial and temporal development of each flash is a more useful and reliable way to identify the sign of the charge regions involved. Since the LMA primarily detects negative breakdown, the propagation direction of the first several sources of a flash are assumed to correspond to negative breakdown that propagates in a direction opposite that of the electric field vector; that is, the lightning mapping of each flash is assumed to initially progress toward positive charge and away from negative charge. Coleman et al. (2003) found good agreement between LMA-inferred charge structure and balloon soundings of electric field. The location of LMA-inferred flash initiation agreed well with the balloon-inferred heights of maximum electric field, and the lightning preferentially branched into wells of electrostatic potential, which are typically coincident with regions of large net charge density. These results from Coleman et al. (2003) support the previously mentioned results from the charge block experiments of Williams et al. (1985) and the modeling studies of Mansell et al. (2002).

To illustrate the LMA-inferred charge structure methodology, Fig. 1 shows lightning mapping of a five-flash sequence during this storm, which reveals five vertically stacked charge regions, alternating in polarity with positive as the lowest. The sources are color-coded by inferred ambient charge region to highlight the stratified structure. Figure 2 shows the second flash of the five-flash sequence, with the sources color-coded by time. The initial negative breakdown of this flash proceeded downward from 9.5 km MSL then through an inferred stratified positive charge region at 8–9 km MSL. A distinct and more sparse grouping of sources above the initiation point mapped out the inferred negative charge at 10–11 km MSL. Additionally, some of the red-colored points late in the flash appear to have retraced the breakdown through both charge regions. Such flashes are termed inverted IC flashes because they reveal an inverted dipole structure. Figure 3 shows the third flash of the five-flash sequence and shares many of the features of the previous flash, but flipped in the vertical. The initial negative breakdown of this flash progressed upward from 8 km MSL into the same stratified positive charge region at 8–9 km MSL that was revealed by the previous inverted flash. The sparse grouping of sources at 6–7 km MSL maps out the inferred negative charge below the positive. Such flashes are termed normal IC flashes as they reveal a normal dipole structure. Hence, the location of the positive charge was consistently revealed by both of these flashes. The remaining flashes of the five-flash sequence in Fig. 1 were similarly clear, with each showing distinct bilevel structure. When put together, they

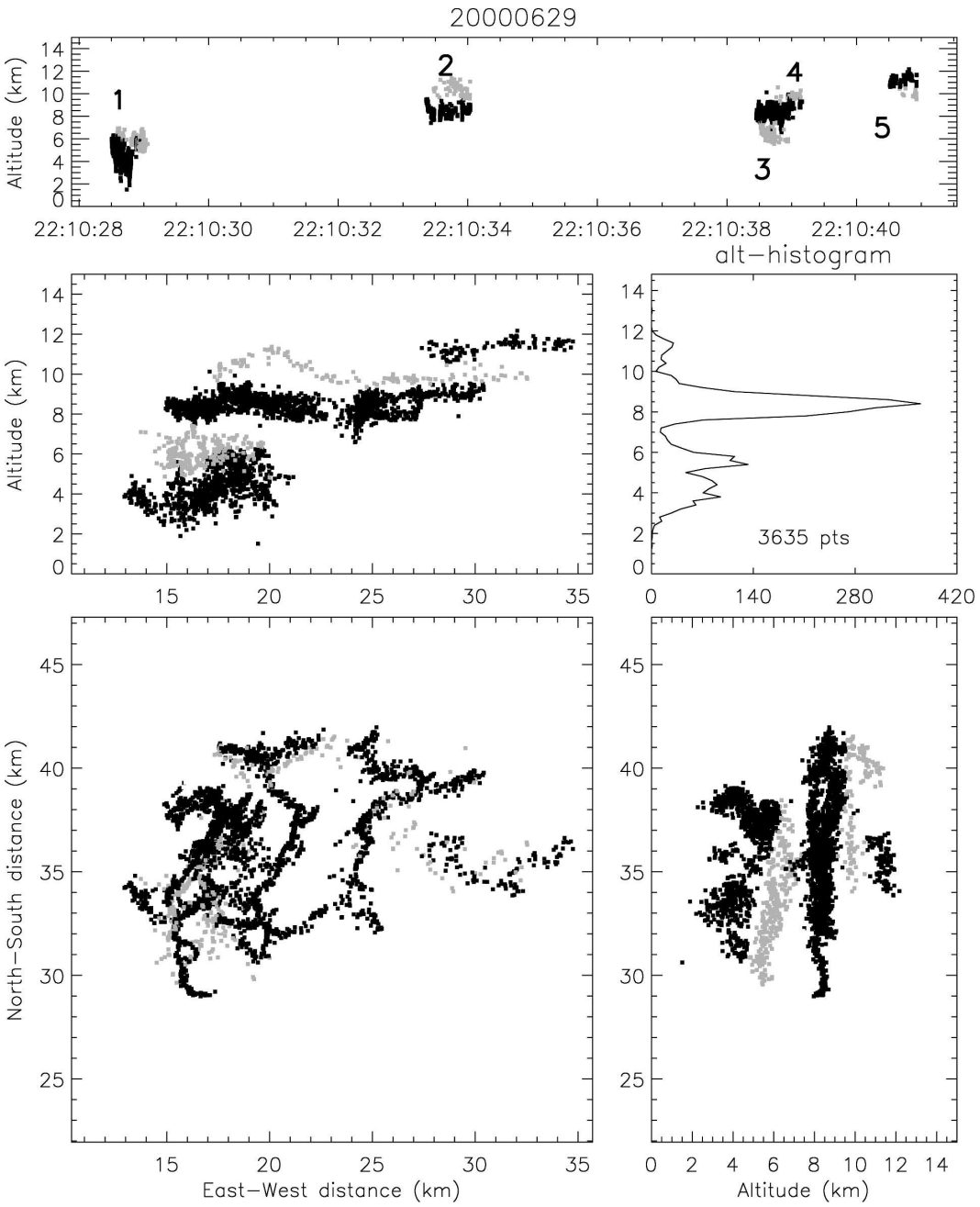

FIG. 1. Lightning mapping of five flashes showing five-layer charge structure at 2210 UTC 29 Jun 2000. (top) Altitude vs time with a label for each flash. (lower) Three different spatial projections along with an altitude histogram of the number of sources. LMA sources are color-coded by inferred ambient charge region, with black for positive and gray for negative. Flashes 1, 2, and 4 are inverted flashes (negative over positive charge). Flashes 3 and 5 are normal flashes (positive over negative).

reveal a very clear and consistent picture of the charge structure.

This sort of flash-by-flash analysis was performed on literally thousands of flashes throughout the duration of this storm. This methodology certainly has limitations, including the following. 1) There is no quantitative information about charge magnitudes. However, distributions of the density of LMA sources can reveal relatively more or less electrically active regions. 2) Sometimes during the severe phase of this storm, distinct charge regions were not always clear. 3) The LMA cannot reveal charge regions that are not involved in light-

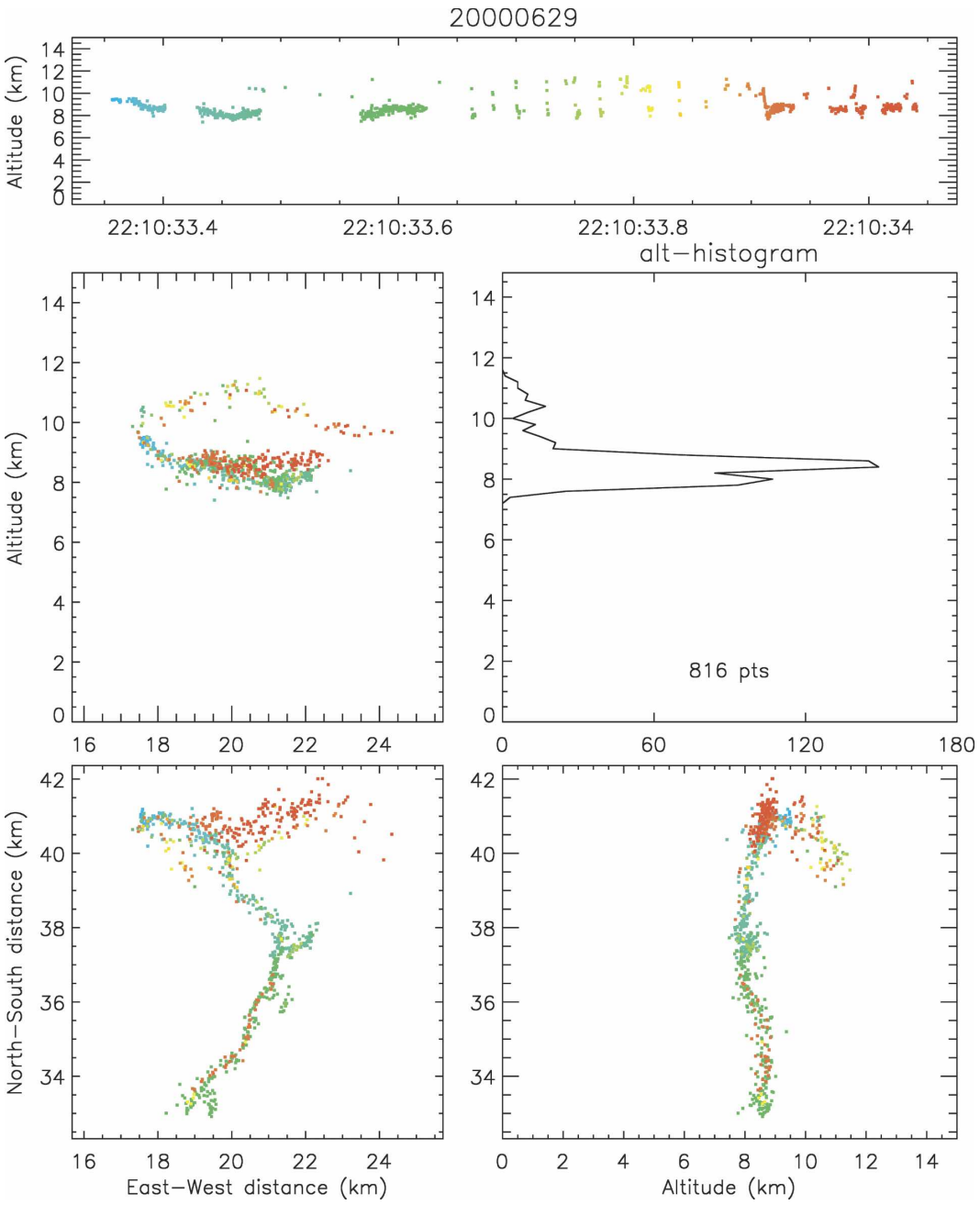

FIG. 2. The second flash of the five-flash sequence in Fig. 1. This is an inverted flash that initiated downward from an inferred ambient negative charge region into an inferred ambient positive charge region. LMA sources are color-coded by time from blue to red.

ning. This method cannot replace in situ measurements. However, it does provide a fully three-dimensional qualitative picture of the charge structure throughout the evolution of the storm to complement the more quantitative information gained from in situ measurements (e.g., balloons and/or aircraft). Furthermore, the development and evolution of charge regions can then be linked to storm dynamical and microphysical processes.

b. Flash rate determination

To determine CG flash rates, the NLDN-identified ground strikes associated with this storm were binned into each UTC minute. Though the leader to ground of

a CG flash is often discernible in the LMA data alone, the NLDN data were compared with the lightning mapping to confirm each ground strike.[1] Total flash rates (IC plus CG) were determined by applying an algorithm developed by Thomas et al. (2003), which sorts LMA data into isolated groups of sources that are separated by less than 150 ms in time and 3 km in horizontal distance. Each group is deemed a flash. All such flashes are then binned into each UTC minute to arrive at a flash rate, that is, total number of flashes in each minute. Williams et al. (1999) and Williams (2001; see his Table 13.2) used a similar method to deduce flash counts from the Lightning Detection and Ranging (LDAR) system at Kennedy Space Center.

This flash sorting algorithm has been tested on storms with low to moderate lightning activity by simply visually counting distinct groupings of LMA points and then comparing the visual count with the output of the sorting algorithm. For these low to moderate cases, the sorting algorithm works very well. However, for more intense storms when the lightning activity is almost continuous (like in the later stages of the storm examined here), it is often impossible to visually discern distinct flashes in the LMA data. Given that there is some uncertainty in the sorting algorithm, there is some concern about the validity of these flash rates. However, for the purposes of this study the interest is primarily in the trends. Figure 4 compares the lightning activity of the 29 June storm in terms of overall LMA sources, total (nonthresholded) flash rates (i.e., all isolated groups of sources, including single-source flashes), and total flash rates that include only those groups of sources with at least 10, 50, and 100 sources. As is evident in this figure, the trends are much the same regardless of how the LMA sources are partitioned into flashes; however, allowing any grouping of sources (including singletons) to be called a flash may lead to the inclusion of noise sources, which could lead to artificially (and unphysically) large flash rates. Imposing the 10-source criterion reduces the nonthresholded total flash rates by a factor of 2–5, while further restricting the flashes to ≥50 or ≥100 sources leads to less severe reduction but very good preservation of the trends in the 10-source metric. The total flash rate (TFR) reported in the remainder of this study corresponds to flashes with ≥10 sources because this seems like a more physically representative metric that is most directly comparable to other flash rates reported in the literature.

3. Observations

a. Overall trends and relationships

To provide some context for the detailed observations that follow, Fig. 5 provides a time series summary of the storm from 2130 UTC (29 June) to 0115 UTC (30 June). Echo volumes of updraft ($w > 10$ m s^{-1}, hereafter UV_{10}), graupel, and hail are plotted in Fig. 5a along with the total volume of the storm (defined as the total echo volume with radar reflectivity in excess of 0 dBZ). To highlight smaller-scale fluctuations, Fig. 5b shows echo volumes of UV_{10}, graupel and hail in terms of their percentage of the total storm volume. Total flash rate (IC plus CG, designated as TFR) and CG flash rates are plotted in Fig. 5c. Overall, IC flashes dominated the lightning activity, with the percent of IC flashes [%IC = IC/(IC + CG)] ranging from 95% to 100%. Of the 254 CG flashes, 223 of them (88%) were positive.[2]

In general, the broad trends in the various echo volume and flash rate time series followed the trend in total storm volume (Fig. 5). The dominant feature of these time series is the dramatic increase in updraft, hail, TFR, and +CG flash rate accompanying the right turn of the storm around 2325 UTC. However, there were several smaller-scale surges. For the most part, each of these surges followed the general pattern of a surge in UV_{10}, followed 5–10 min later by coincident surges in graupel echo volume and TFR, followed 5–10 min later by surges in hail echo volume. Surges in updraft affected the vertical distribution of reflectivity and lightning as well (Fig. 6). Bursts of updraft (thick blue line in Fig. 6b) generally led to greater vertical extent of both significant reflectivity and lightning. For example, note in Fig. 6 that during the first 15 min of the obser-

[1] In practice, we actually first look at the time and location of an NLDN ground strike, then see if the LMA data corroborate the NLDN. According to Cummins et al. (1998), +CG flashes with peak currents less than 10 kA may in fact be intracloud flashes that the NLDN misidentifies as +CG flashes. They recommend that such low current +CG flashes be treated with suspicion. The only +CG flashes in the 29 June 2000 storm with peak currents between 5 and 15 kA occurred during the volume scan beginning at 2252 UTC. The lightning mapping of these two +CG flashes (not shown) suggests that they were, in fact, intracloud flashes. These two suspicious +CG flashes were thus removed from consideration.

[2] As discussed in Part I, a separate smaller cell formed near 2400 UTC, just northwest of the supercell of this study. It produced some hail and frequent lightning (though nowhere near the scale of the supercell), and dissipated by 0100 UTC. Calculations of flash rates and echo volumes include this separate cell. It produced only six CG flashes (five negative and one positive), all of which occurred as it collapsed during the 0056 UTC volume scan.

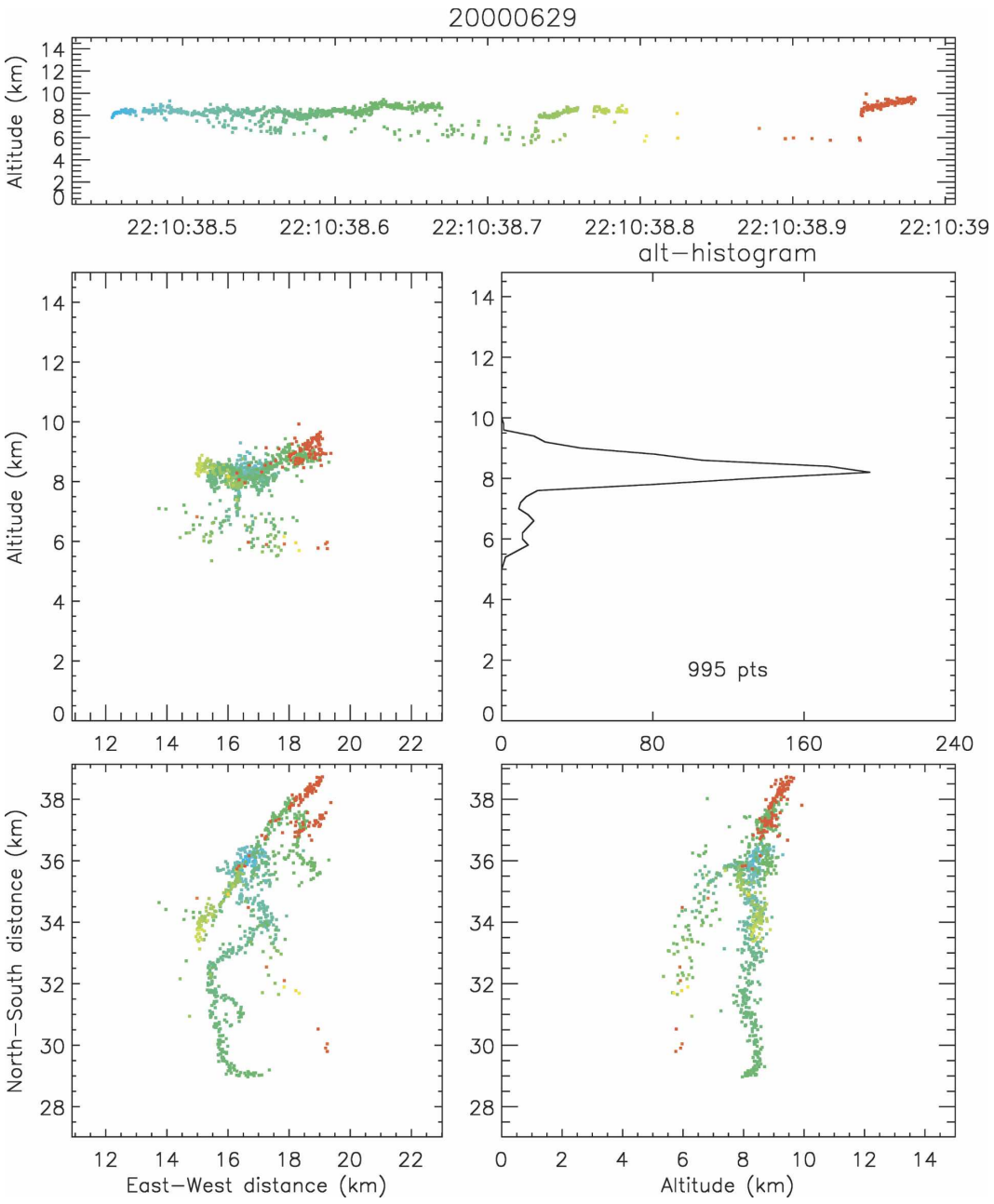

FIG. 3. The third flash of the five-flash sequence in Fig. 1. This is a normal flash that initiated upward from an inferred ambient negative charge region into an inferred ambient positive charge region. LMA sources are color-coded by time from blue to red.

vation period (2130 to 2145 UTC), the updraft was small in terms of both magnitude and volume. Consequently, there was little graupel volume above 8 km, and the lightning activity was entirely below an altitude of 8 km (highly concentrated near 5 km). Following a burst of updraft around 2144 UTC, the lightning became highly concentrated at higher levels in an elevated reflectivity feature and the flash rate increased substantially. As time progressed, the precipitation volumes and lightning pulsed in vertical extent in apparent response to bursts in updraft, with the density of LMA sources closely tracking graupel echo volume in both time and height (cf., e.g., the contours of graupel echo volume to those of LMA sources in Fig. 6). On a few occasions, strong bursts of updraft led to numerous LMA sources (from tens to hundreds of sources, or 15–25

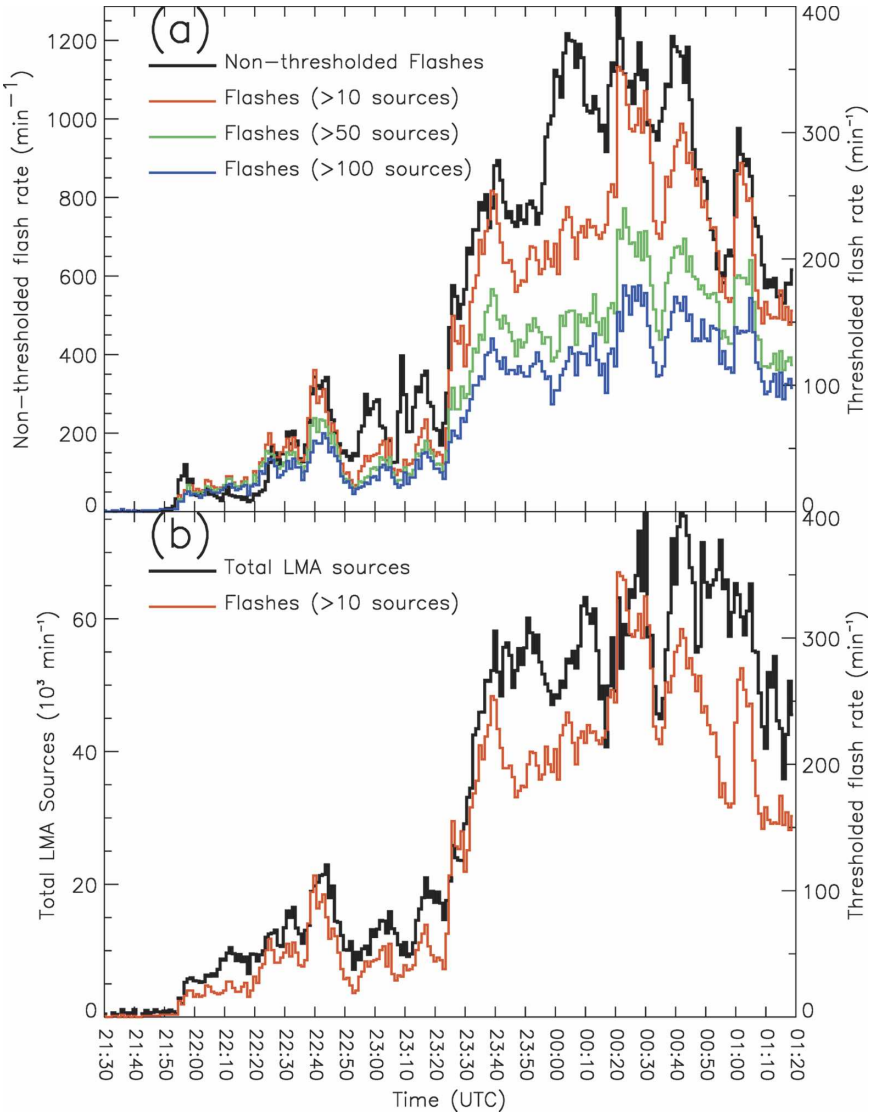

FIG. 4. Comparison of LMA metrics of lightning intensity. Each of these plotted quantities represents the total count of each category binned into each even UTC minute, i.e., not averaged in any way. (a) Total (nonthresholded) flashes each minute (black) compared with flashes having at least 10 (red), 50 (green), and 100 (blue) sources. Note the separate ordinate axes for thresholded and nonthresholded flashes. (b) Total LMA sources each minute (black) compared with flashes having at least 10 sources (red). Note the separate ordinate axes for total LMA sources and flashes. Total (nonthresholded) flashes include all isolated groups of LMA sources (including single-point events). The TFR discussed in the text corresponds to the 10-source thresholded category of this figure. The TFR is plotted as the average over the 5–7-min interval of the radar volume scans in Fig. 5.

dB min^{-1}) extending as high as 15 km MSL (see, e.g., around 2330 and 2400 UTC in Fig. 6). Such vertically elevated LMA sources in response to convective surges have also been documented by Hamlin et al. (2001) and Hamlin (2004). Throughout the last 3 h of the observation period, there was considerable lightning activity at all altitudes below 15 km. However, the highest concentration of LMA sources, and thus the highest likely concentration of positive charge, remained at a relatively steady altitude centered near 8 km MSL ($T \approx -12$°C). There were also surges in the +CG flash rate, and these surges generally occurred during dramatic intensification of the storm's updraft and hail production. For example, the first two +CG flashes occurred near the time (2239 UTC) of relative maxima in TFR and hail echo volume. There were no +CG flashes and

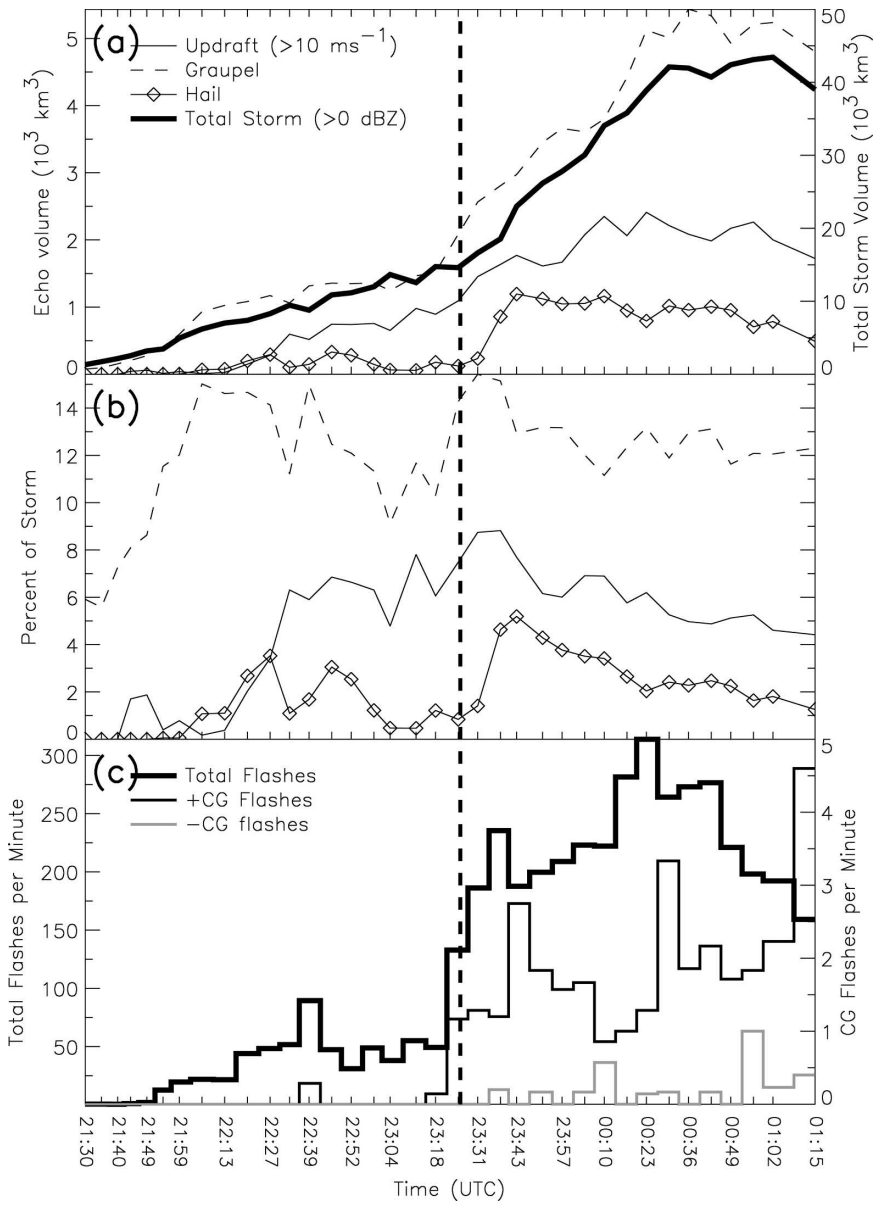

FIG. 5. Time series summary. (a) Radar-inferred echo volumes of storm updraft ($w > 10$ m s^{-1}, UV_{10}), graupel, and hail. Thick black line shows total storm volume (defined as volume of storm with radar reflectivity exceeding 0 dBZ). (b) As in (a), but with echo volumes plotted as percent of total storm volume. (c) TFR and CG flash rates averaged over each radar volume scan time interval. TFR includes only those flashes with at least 10 sources in each flash (see Fig. 4). Each tick mark on the time axis indicates the start time of a radar volume scan. Vertical dashed line indicates the time (2325 UTC) when the storm made a right turn.

little hail echo volume from 2252 to 2318 UTC. Then, at 2325 UTC, as the hail echo volume began to increase dramatically, so did the +CG flash rate. However, near the end of the observation period (0115), the UV_{10}, and hail echo had been declining steadily, while the +CG flash rate reached its absolute maximum of the entire observation period.

In an attempt to quantify the relationships among updraft, precipitation, and lightning, residual correlation analyses were performed on their respective time series. Since the bulk of the variance in all the time series of Fig. 5 can be accounted for by the steady quasi-linear increase in total storm volume (see the first column of Table 1), the correlations were isolated from the dominating influence of the total storm volume. In mathematical terms, each of the raw time series (e.g.,

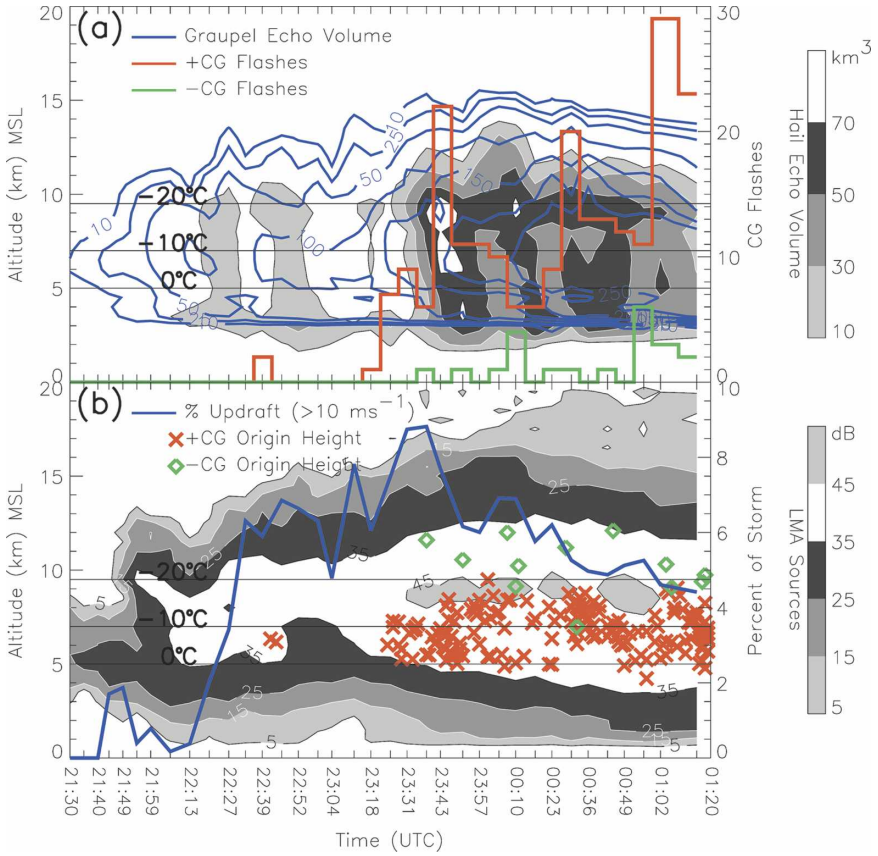

FIG. 6. (a) Contours of the number of radar grid points at each time and height classified as hail (in grayscale) and graupel (blue). The number of grid points has been multiplied by the dimensions of a grid cell (0.5 km)^3, resulting in units of echo volume. The total number of +CG and −CG flashes during each volume scan are plotted in red and green, respectively. Here, the CG flashes are summed (not averaged) over the duration of each volume scan. (b) Time–height contours of total LMA sources (in grayscale) normalized to a 5-min time interval. Contour values are in decibel units [i.e., $10 \log_{10}$(# sources)] due to the large range of magnitude. The percent volume of updraft exceeding 10 m s^{-1} is overlaid onto (b) as a thick blue line. Origin altitudes of +CG and −CG flashes are overlaid onto (b) as red ×'s and green diamonds, respectively.

UV_{10}, graupel, TFR) was separately least squares fit to the total storm volume time series. The fitted time series were then subtracted from the raw series to get the detrended residual time series, which are, by definition, uncorrelated to the total storm volume. The correlation coefficients between the residual time series were then computed as a function of lag.[3] Figures 7 and 8 show graphical representations of this procedure, and Table 1 summarizes the results.

Several studies (e.g., MacGorman et al. 1989; Carey and Rutledge 1996) have shown that TFR is very well correlated with the volume of 30–40-dBZ radar reflectivity within the mixed-phase region (often called the Larson Area; Larson and Stansbury 1974) where collisional charging is thought to occur. This Larson Area essentially describes the same thing as does our graupel echo volume, and we find a similar result for this storm. The TFR shows a robust correlation with graupel echo volume (and with UV_{10}, to a lesser extent) even after the influence of the total storm volume has been removed (Fig. 9). Note that the residual correlation between graupel and TFR peaks at zero lag (Fig. 8). That is, the best correlation between these two residual time series occurs when the time series are contemporane-

[3] MacGorman et al. (1989) used a similar detrending procedure; however, instead of removing the variance explained by the large-scale trend in overall storm volume, MacGorman et al. removed the separate linear trend of each of their time series prior to computing correlations.

TABLE 1. Correlation coefficients between radar and lightning time series. Values outside of parentheses give correlations between zero-lag time series, prior to any trend removal. Values in parentheses give correlations between detrended time series at zero lag. Additional correlation coefficients and lag values are given if the best detrended correlation occurred at nonzero lag. Each lag increment corresponds to one 5–7-min radar volume scan interval. For example, the best detrended correlations for the +CG flash rate time series occurred when the +CG flash rate lagged the updraft, graupel, and TFR time series by one scan interval, but led the hail time series by two scan intervals.

	Total storm volume	Updraft volume (>10 m s^{-1})	Graupel echo volume	Hail echo volume	Total flash rate
Updraft	0.95				
Graupel	0.99	0.95 (0.23)			
Hail	0.84	0.89 (0.53) (0.57@−1)	0.85 (0.24) (0.73@−2)		
Total flash rate	0.90	0.95 (0.68)	0.95 (0.84)	0.90 (0.58) (0.75@+2)	
+CG flash rate	0.81	0.76 (−0.02) (0.31@−1)	0.81 (0.08) (0.58@−1)	0.72 (0.10) (0.67@+2)	0.74 (0.04) (0.52@−1)

ous. This is true for UV_{10} versus TFR as well (Fig. 8). However, the correlation versus lag for UV_{10} and TFR is not as sharply peaked as it is for graupel and TFR. The UV_{10} versus TFR correlation decreases more gradually when TFR lags UV_{10} and more sharply when UV_{10} lags TFR. This makes physical sense. Increases in the volume of significant updraft should lead, after some delay, to increases in graupel formation, electrification, and flash rate.

None of the other pairs of time series shows such strong contemporaneous residual correlations; however, there are some interesting results at nonzero lag (see Table 1). The hail volume is best correlated with UV_{10}, graupel, and TFR when it lags the UV_{10} by one volume scan interval (5–7 min) and lags the graupel and TFR by two volume scan intervals (10–15 min). The +CG flash rate is not well correlated with any other quantity at zero lag, and the best correlations between +CG flashes and the other quantities occur when +CG flashes lag graupel, UV_{10}, and TFR but lead hail. One interpretation of these collective results is that the broad, strong updrafts led rapidly to increased graupel and increased charge-separating collisions involving this graupel. With time, the graupel continued to grow within the supercooled liquid water–rich updrafts, forming hail. The lagged correlation between TFR and hail (and weaker correlation overall) seems to support the idea that hail plays a minimal role in charge sepa-

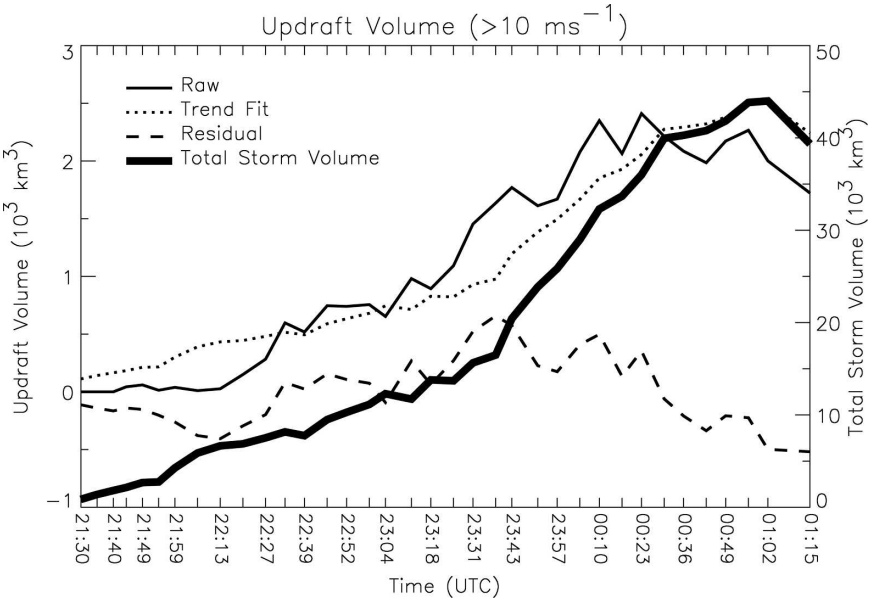

FIG. 7. Graphical example of the time series detrending procedure. In this example, the time series is updraft volume exceeding 10 m s^{-1} (UV_{10}). A linear least squares fit of the raw time series to the total storm volume time series gives the trend fit. The trend fit is then subtracted from the raw time series to give the residual (detrended) time series.

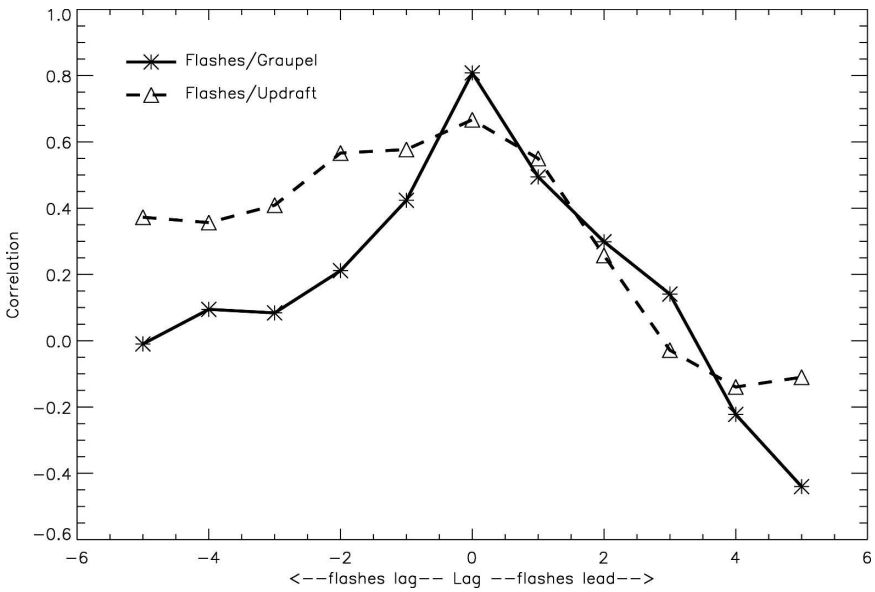

FIG. 8. Correlation coefficients as a function of lag for two pairs of residual time series: graupel echo volume vs TFR and UV_{10} vs TFR. A positive (negative) lag indicates that the TFR time series leads (lags) the graupel or UV_{10} time series. Each lag increment corresponds to the time interval (5–7 min) between successive radar volume scans. The actual residual time series are plotted in Fig. 9.

ration. As discussed in Williams (2001), hail is unlikely to be a major player in charge separation because of its minuscule integrated surface area available for collisional charging (compared to an equivalent mass of graupel). Furthermore, in a high liquid water content regime, hail has a tendency for wet growth. Saunders and Brook (1992) found that there is insignificant charge transferred by the noninductive process in wet growth conditions.

Though we hesitate to attach too much significance to these results, the TFR (and to a lesser extent, +CG flash rate) seemed to be a good indicator of this storm's intensification and may have some utility as a predictor of severe weather in the form of hail. Williams et al. (1999) found a similar result in their comparison of radar-inferred storm development to total flash rates derived from the LDAR system at Kennedy Space Center. They found that total flash rate would often jump dramatically during explosive vertical development of the radar echo, and these lightning jumps were typically followed tens of minutes later by severe weather at the ground in the form of hail and downbursts.

To reveal the relationships among +CG flashes, updraft strength, and hail production, we need to know not just when but also where in the storm the +CG flashes originated and where they struck ground. To this end, the LMA data were used to extract the origin location of CG flashes. Similar to Proctor (1991), the origin location of each CG flash was defined as the centroid of the first 10 LMA sources associated with the flash. (There were typically hundreds to thousands of sources in each CG flash.) Origin heights were determined for 180 of the 254 total CG flashes identified by the NLDN during the observation period. The discrepancy between the numbers of CG flashes and CG origin heights is for two reasons. 1) An origin location for a CG flash was determined only if its associated LMA sources could be clearly isolated and extracted from the surrounding lightning activity. 2) As in Lang et al. (2004b), there were several instances in which multiple CG strike points originated from the same LMA-mapped parent flash. Each of the strike points is considered a separate CG flash by the NLDN as well as in the CG flash rate time series of this study. However, since these multiple strike points originated from the same flash, they were assumed to share a common origin for the purposes of computing the mean origin height. Figure 10 shows an altitude histogram of these CG flash origin heights, for both positive and negative polarity CG flashes. The CG origin heights are also overlaid onto the time–height contours of Fig. 6b. The +CG flash origin altitudes were generally constrained between 5 and 9 km MSL with a mean origin altitude of 6.8 km (temperature range of 0° to −20°C, centered near −10°C). This height range was clearly in the low to

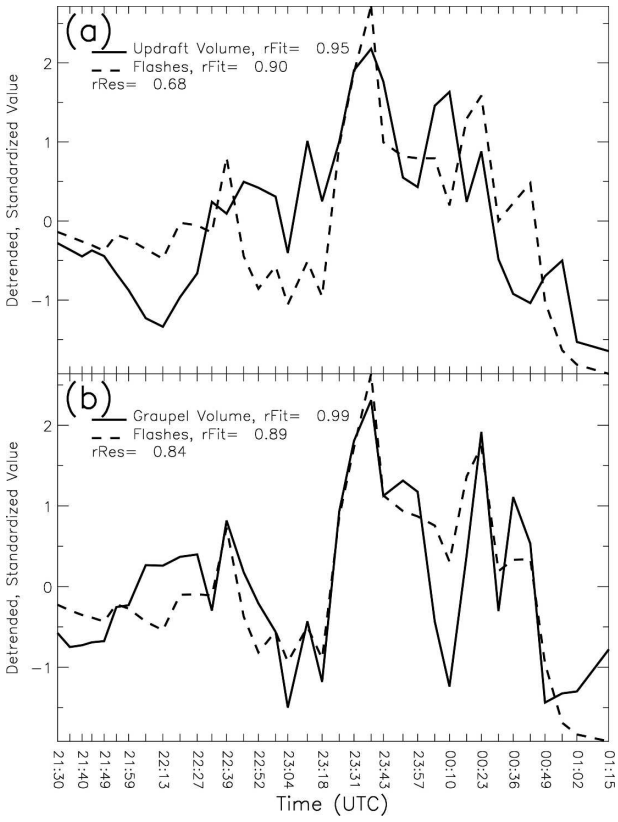

FIG. 9. Residual time series of (a) UV_{10} and TFR and (b) graupel echo volume and TFR. The "rFit" numbers give the correlation coefficient between the raw time series and the time series of total storm volume, while the "rRes" numbers give the correlation coefficient between the two plotted residual time series.

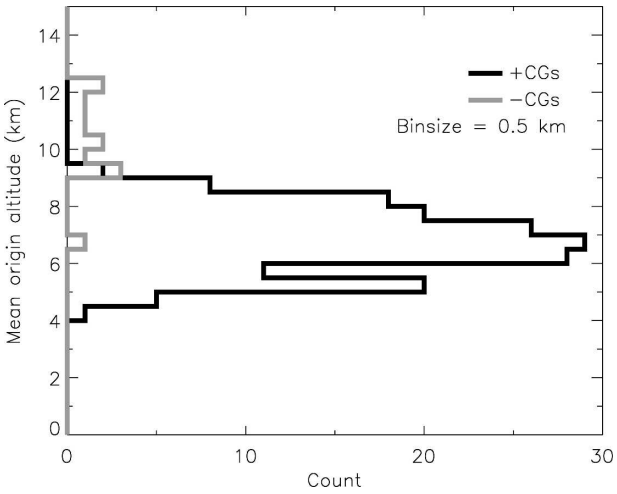

FIG. 10. Histogram of mean LMA-inferred CG origin altitude, i.e., mean altitude of the first 10 LMA sources of each CG flash.

midlevel of the storm, not the anvil region. In contrast, all but one of the −CG flashes originated from >9 km MSL, that is, above where the +CG flashes originated. Though there is some scatter, during any given volume scan time interval the mean of the +CG flash origin heights was between 6 and 7.5 km, which is consistent with the region of dense positive charge implied by the LMA density contours in Fig. 6b. Radar-inferred hail and graupel were both highly concentrated in the inferred +CG flash origin height region. There were no +CG flashes without the presence of radar-inferred hail somewhere in the storm; however, this alone does not imply any horizontal relationship between hail and +CG flashes.

b. Detailed observations of lightning and charge structure

To illustrate the evolution of precipitation and electrical structure in the storm, Figs. 11–13 show representative horizontal and vertical cross sections of radar reflectivity and LMA source density during selected volume scans, along with a composite schematic of the charge structure inferred from lightning mapping of many individual lightning flashes. The LMA density plots in these figures are not exactly cross sections per se. They count up all the LMA sources within a swath centered on the cross-section plane. For example, in the horizontal cross sections at (z = 7 km), the LMA density plots sum all the LMA sources from 4.5 to 9.5 km (i.e., 7 ± 2.5 km), while the vertical cross sections sum all the LMA sources within ±5 km of the vertical cross-section plane. These LMA density plots give an objective depiction of the electrically active regions of the storm, while the charge composites provide a somewhat more subjective interpretation of these regions. We must stress that during the later severe phases of this storm, the lightning was very frequent and the LMA-inferred charge structure was not always clear. Thus, the charge composites are likely incomplete and oversimplified, but they do capture the gross charge structure revealed by the majority of the lightning flashes.

1) DEVELOPING PHASE (2130–2213 UTC)

Over the first 20 min of the observation period (2130 to 2150 UTC), the storm consisted of a disorganized line of convective cells aligned roughly southwest–northeast near the Colorado–Kansas–Nebraska border. New cells developed to the west with precipitation forming and descending to the east of the updraft. The westernmost of these cells developed into the storm of this study. The lightning was relatively infrequent (1–2 flashes per minute), and consisted entirely of IC flashes between an inferred negative charge region at an alti-

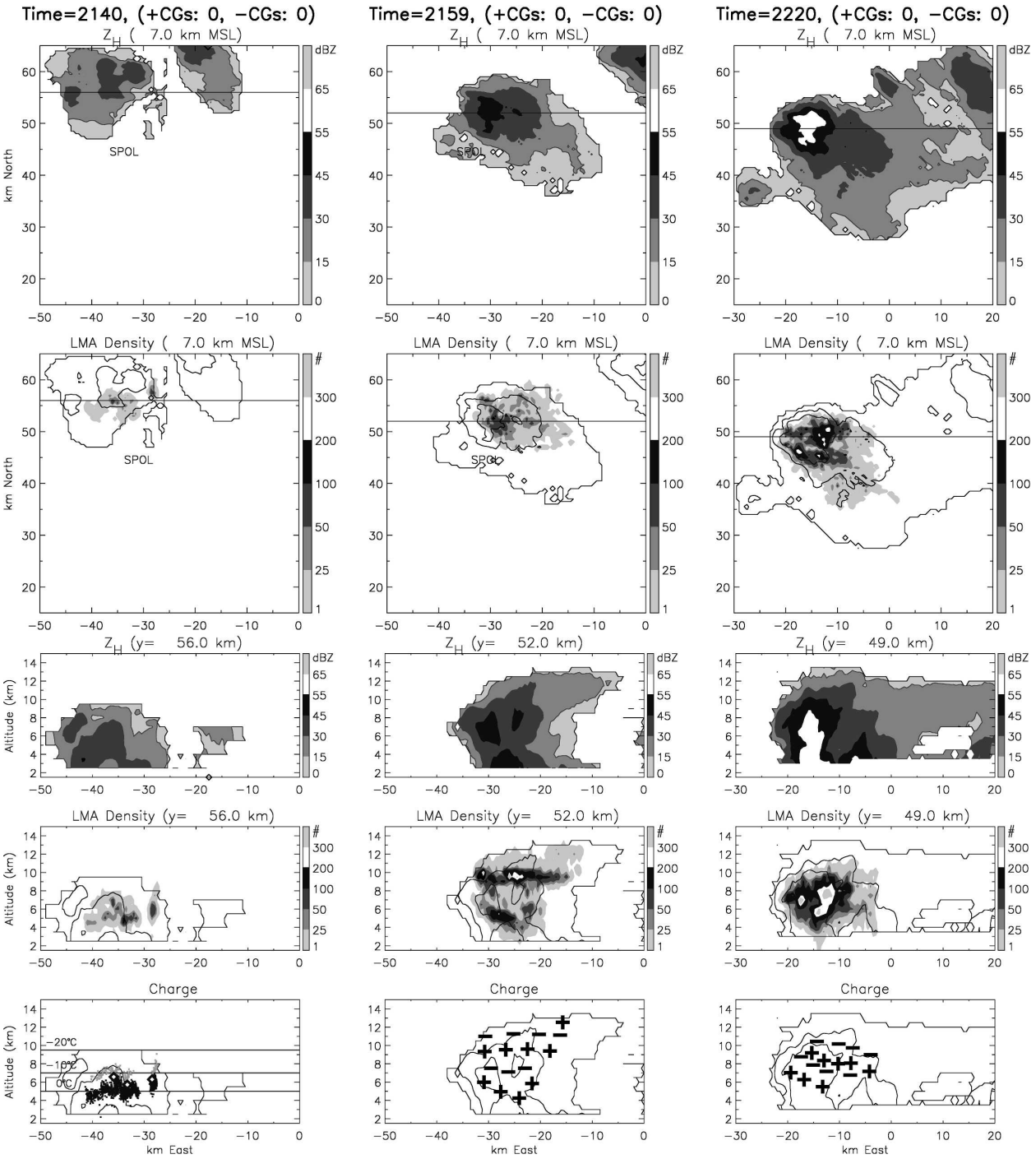

FIG. 11. Representative cross sections for volume scans beginning at 2140, 2159, and 2220 UTC. Each column corresponds to the same time. (top two rows) Horizontal cross sections of radar reflectivity (Z_H) and LMA source density at 7-km altitude. (third and fourth rows) East–west vertical cross sections of the same quantities along the lines indicated in the top two rows. LMA source density plots show the number of sources (#) within 2.5 (5.0) km of each horizontal (vertical) cross section. (bottom row) LMA-inferred charge structure at each time. For 2140 UTC, the LMA sources from the three flashes during this volume scan are overlaid and color-coded by charge, with black (gray) indicating inferred ambient positive (negative) charge region; filled diamond symbols indicate the first source of each flash. For all other times, the charge structure is a composite schematic; Z_H contours are repeated on the LMA and charge structure plots, with intervals of 0, 30, and 45 dBZ.

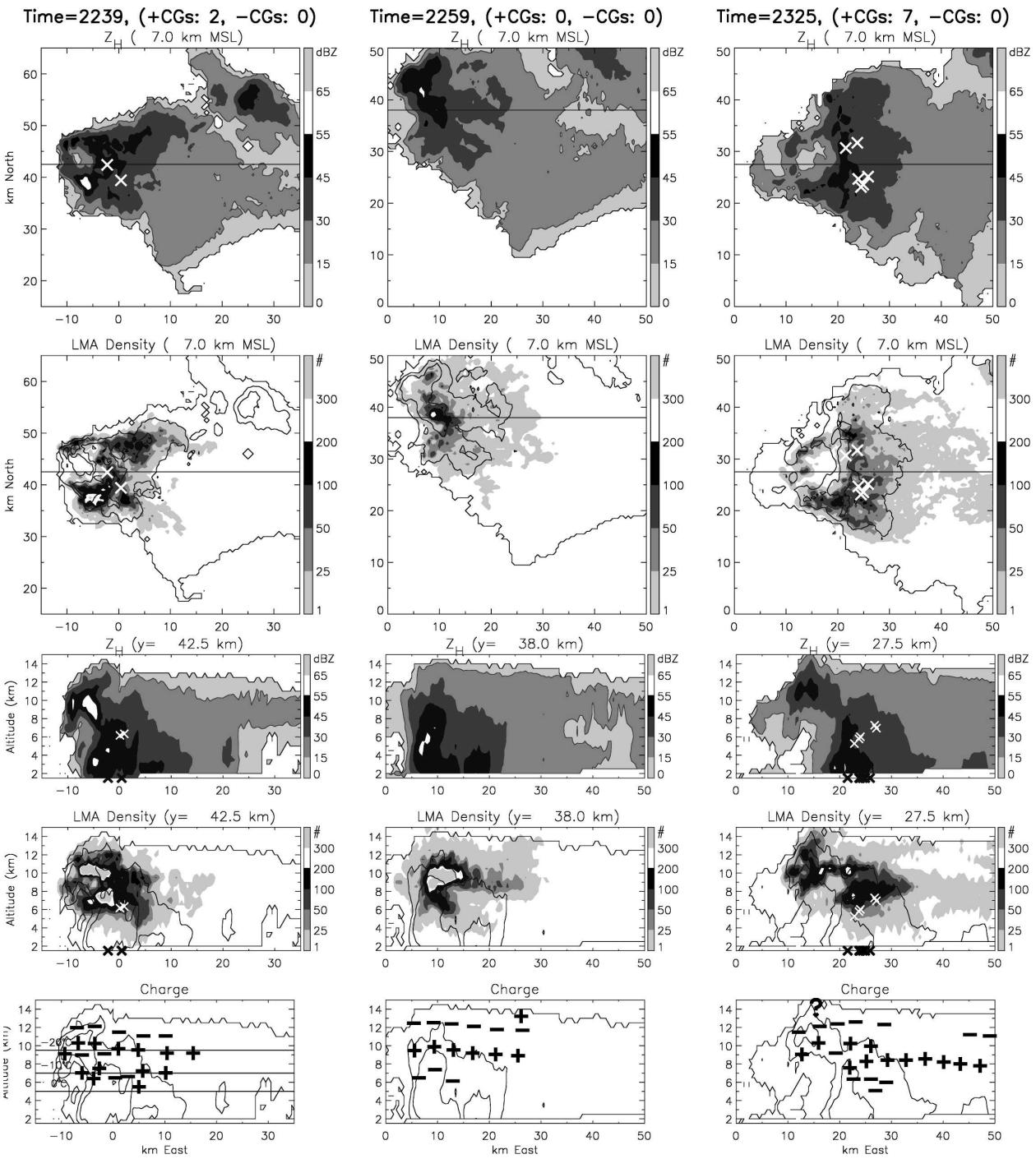

FIG. 12. As in Fig. 11, but for volume scans beginning at 2239, 2259, and 2325 UTC. In addition, the × symbols on the horizontal cross sections and along the bottom of the vertical cross sections indicate the NLDN strike locations of +CG flashes. The × symbols at higher altitudes on the vertical cross sections indicate the LMA-inferred origin locations of +CG flashes. Only those CG flashes that struck within 5 km of the cross-section plane are shown on the vertical cross sections. Color of CG strike and origin symbols varies only to provide sufficient contrast against gray-shaded background contours.

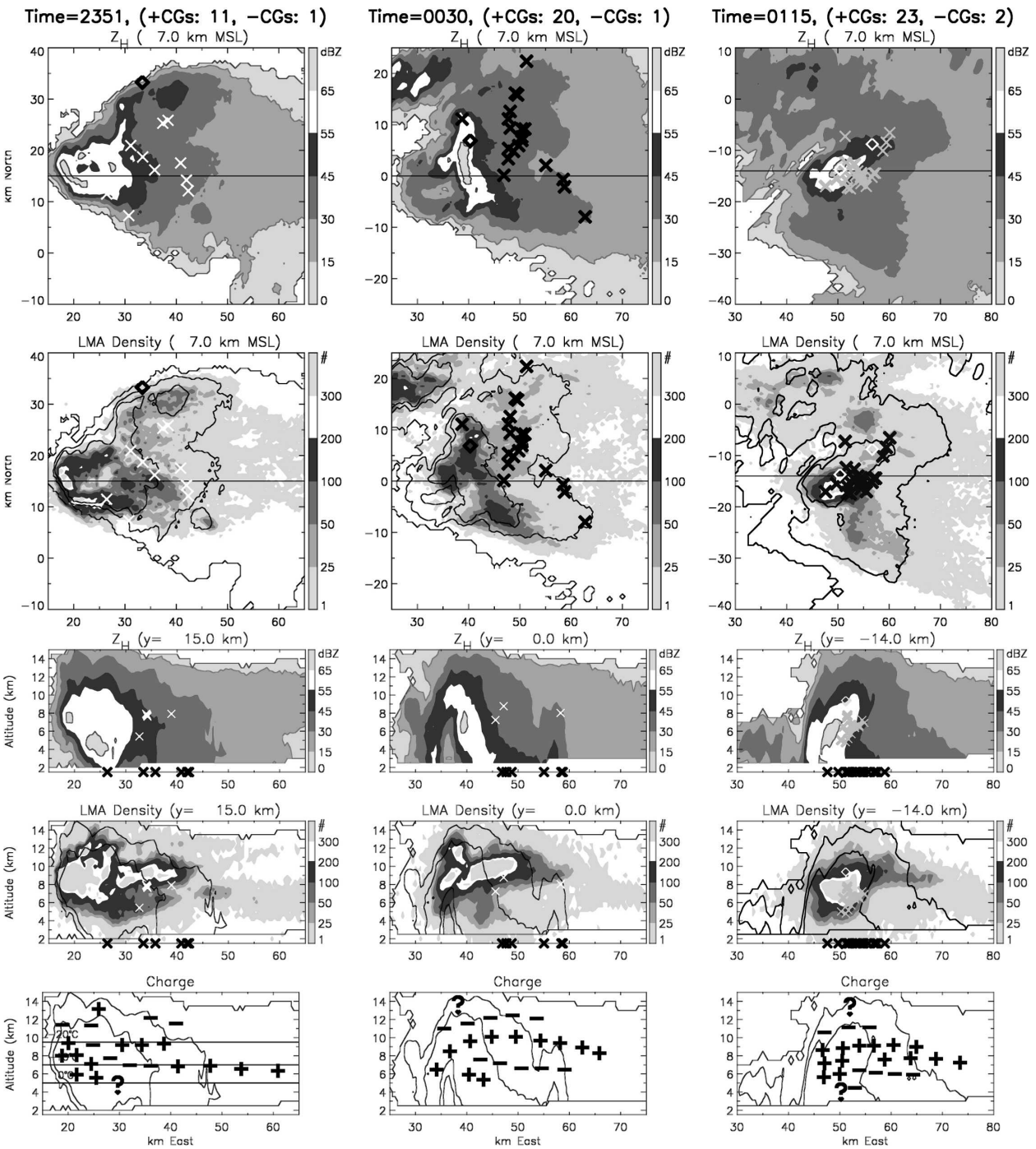

FIG. 13. As in Fig. 11 but for volume scans beginning at 2351, 0030, and 0115 UTC. Origin and strike locations of CG flashes are indicated as in Fig. 12, with −CG flashes indicated by diamond symbols.

tude of 7–8 km ($-10° < T < -15°$C) and a lower positive charge region at 4–5 km ($T \approx 0°$C). These IC flashes tended to originate in the elevated precipitation east of the updraft; they then propagated down through the inferred lower positive charge region associated with descending precipitation. The three flashes that occurred from 2140 to 2144 UTC are representative of this early lightning activity. Their LMA sources are overlaid onto the bottom-left panel of Fig. 11. This arrangement of charge could be described as an inverted dipole; however, the two charge regions involved in this early lightning activity might correspond to the lowest

two charge regions of the tripole model and Stolzenburg et al. (1998a,b,c) observations. This early charge structure departed from the tripole model in that there was no lightning activity indicative of a positive charge region above the negative charge.

During the radar volume scan beginning at 2144 UTC, the storm developed a strong, broad, rotating updraft on its northwestern edge, with speeds exceeding 20 m s^{-1} at an altitude of 10 km. Prior to this, updrafts did not exceed 6 m s^{-1}. In apparent response to this updraft burst, the storm developed a region of elevated reflectivity aloft and, by 2154 UTC, began producing frequent (tens per minute) inverted IC flashes between a negative charge region at an altitude near 11 km and a positive charge region at 9–10 km. This rapid transition to frequent upper-level flashing is evident in the time series and contours of Figs. 5c and 6b. In addition to these upper-level flashes, the storm continued to produce relatively infrequent IC flashes between the midlevel negative and lower positive charge regions, with the LMA sources sometimes extending to altitudes as low as 3 km. There were also infrequent compact discharges at even higher altitudes (between negative charge at 12 km MSL and positive charge at 13 km). These extremely elevated discharges tended to be well downwind of the updraft in the low reflectivity anvil region of the storm and may have been indicative of a positive screening layer on the upper cloud boundary. Hence, overall the LMA-inferred charge structure consisted of a lower inverted dipole, an upper inverted dipole, and an additional positive charge at the top. Figure 14 shows lightning mapping of five successive flashes (from 2200:46 to 2200:59 UTC) that spanned these five inferred charge regions. As illustrated by the charge composite and vertical cross section of LMA source density in Fig. 11 (second column, bottom two panels), the lightning flashes from 2155 to 2210 UTC were all consistent with this basic five-layer structure. Most of the flashes occurred in the charge regions of the upper inverted dipole, leading to a pronounced peak in LMA source density in the upper positive charge, with a secondary peak corresponding to the positive charge of the lower inverted dipole. Until 2210 UTC or so, the lightning flashes in the upper inverted dipole remained distinctly separate from those in the lower inverted dipole, with no flashes connecting the two regions. The most important point to note, however, is that the upper-level lightning activity formed as a result of invigorated updraft and revealed an inverted dipole. This storm maintained a roughly inverted dipole charge structure within the strongest updraft throughout the observation period, with fleeting evidence of additional extreme upper positive charge.

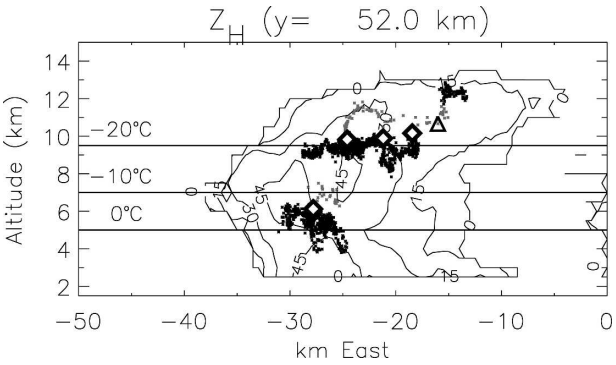

FIG. 14. Vertical cross section of radar reflectivity (Z_H) along y = 52 km for volume scan beginning at 2159 UTC; Z_H contour intervals are 0, 30, and 45 dBZ. LMA sources from five successive and representative individual flashes from 2200:46 to 2200:59 UTC are overlaid and color-coded by inferred ambient charge region with black for positive and gray for negative. Filled triangle (diamond) symbols indicate the first sources of upward (downward) initiating flashes. There are four downward flashes and one upward flash.

Another feature of the early lightning activity warrants some discussion. The presence of a lower charge region is thought to provide the bias for discharges to propagate to ground as CG flashes (e.g., Jacobson and Krider 1976; Williams 2001; Mansell et al. 2002; Marshall and Stolzenburg 2002). That is, −CG (+CG) flashes are more energetically favorable if there is lower positive (negative) charge, which could initiate a downward discharge from a larger negative (positive) charge above it. During the first hour of lightning activity in this storm, there were no CG flashes of either polarity even though the LMA data strongly suggest the presence of a lower positive charge region beneath a negative charge region. Presumably the magnitudes of the negative and lower positive charge regions differed from those of the more commonly observed tripole, such that IC flashes between these regions were more energetically favorable than −CG flashes (Marshall and Stolzenburg 2002). There was also no apparent negative charge region below the lower positive to provoke a +CG flash. There were no in situ electric field measurements taken in the storm during this early lightning period so the magnitudes of the charge regions are unknown, and there is no information about the presence of negative charge below the below the positive charge. The LMA did not indicate any such lower negative charge region.

2) MATURE PHASE (2213–2325 UTC)

As described in Part I, there were two periods of hail growth and fallout during the mature phase (2213–2325 UTC), the first associated with the updraft surge begin-

ning at 2144 UTC giving a hail echo maximum at 2220–2227 UTC, and the second associated with a larger updraft surge that began at 2220 UTC and persisted for 30 min (Fig. 5). The vertical distribution of lightning activity followed the growth aloft and descent of the precipitation during each of these periods (Fig. 6).

From 2159 to 2213 UTC, as the updrafts waned and the lofted precipitation grew and descended, the lightning continued to show five-layer charge structure (e.g., Fig. 1), though more compressed. There were also more normal IC flashes connecting the negative charge of the lower inverted dipole to the positive charge of the upper inverted dipole (e.g., Fig. 3). In other words, the two dipole charge regions no longer remained separate. However, flashes in the upper inverted dipole still dominated the lightning activity. By 2220 UTC, there was still some semblance of a four-layer alternating charge structure. However, the charge regions were more compressed with a pronounced downward sloping east-southeastward away from the updraft (Fig. 11, third column, bottom two panels). The lower positive charge was more restricted near the precipitation core, as if the largest hydrometeors were carrying this lower positive charge with it to ground, while the charge (presumably carried by smaller particles) in the next three alternating regions (negative/positive/negative) sloped downward more gradually further downwind. Indeed, the lower negative charge formed a very low-level (4–5 km) stratified layer extending well southeast of the bulk of the lightning activity. This southeastward extension is not apparent in the vertical cross sections in the third column Fig. 11 (because the associated LMA sources are too far away from the cross-section plane to be included in the plot) but can be inferred from the horizontal cross section in the second panel.

Following another surge in updraft, a resurgence of lightning at upper levels (≈8–12 km MSL) began around 2227 UTC (Fig. 6). By 2239 UTC the TFR reached a peak of nearly 100 min^{-1} (Fig. 5). As described in Part I, a bounded weak echo region (BWER) had developed in association with the strong updraft on the western edge of the storm. The lightning activity mirrored the reflectivity structure of this BWER, with almost no lightning activity within the BWER (constituting a midlevel lightning hole, for lack of better term) and very active lightning in the strong lofted echo above and to the south of the BWER (Fig. 12, left column). The lightning was very frequent, making LMA-based charge structure determination much more difficult. However, the vast majority of the flashes near and within the echo vault surrounding the BWER were inverted IC flashes, leading to the inference of a four-layer alternating charge structure near the main updraft. The positive charge regions of this structure correspond to the two prominent peaks of LMA source density in the vertical cross section of Fig. 12 (left column, bottom two panels). As at 2220 UTC, the upper-inverted dipole persisted downwind (east-southeast) and sloped downward, while the charge structure in the lower part of the storm was more complex (or at least more difficult to determine). However, there was a handful of normal IC flashes to the near southeast of the precipitation core revealing positive charge at 6.5–10 km MSL and negative charge below (e.g., Fig. 15). The first two +CG flashes of the storm (Fig. 16) originated from the same region as these normal IC flashes (though on the northwest edge of this region), and struck ground just southeast of the surface hail swath. Prior to their return strokes, the structure of these two +CG flashes was very similar to the preceding normal IC flashes shown in Fig. 15. That is, the initial negative breakdown of both the normal IC and the +CG flashes progressed upward, defining positive charge at 6.5–10 km MSL, with later breakdown below the initiation point through negative charge below. Additionally, the +CG flashes also appeared to tap some positive charge further west within the precipitation core and echo vaults surrounding the updraft. The storm did not produce any more CG flashes of either polarity until the onset of the severe right mature phase at 2325 UTC.

From 2246 to 2252 UTC, hail continued to grow and descend giving a deep hail shaft and relative maximum in hail echo at 2246 UTC (Fig. 6). TFR decreased to 50 min^{-1}. As shown in Fig. 17, the lightning tended to avoid the >55 dBZ hail shaft almost entirely during this time, again suggesting that hail plays a minimal role in charge separation. By 2259 UTC, the hail had almost all fallen out, and the bulk of the lightning activity was again nearer the precipitation core, but was very concentrated above the collapsing hail shaft (Fig. 12, middle column). Overall, the LMA indicated an inverted tripole with inferred positive charge region centered at 8–10-km altitude and negative charge regions above and below. Though a lower negative charge was present beneath the midlevel positive, this charge structure did not produce +CG flashes. During the brief decline in updraft and hail volumes preceding the onset of the severe right mature phase at 2325 UTC, the storm maintained this gross inverted tripole structure.

3) SEVERE RIGHT MATURE PHASE (2325–0036 UTC)

The storm and charge structure at the beginning of the severe right mature phase (2325 UTC) was in many ways similar to that at 2239 UTC. A strong, broad updraft on the western flank was coincident with an echo

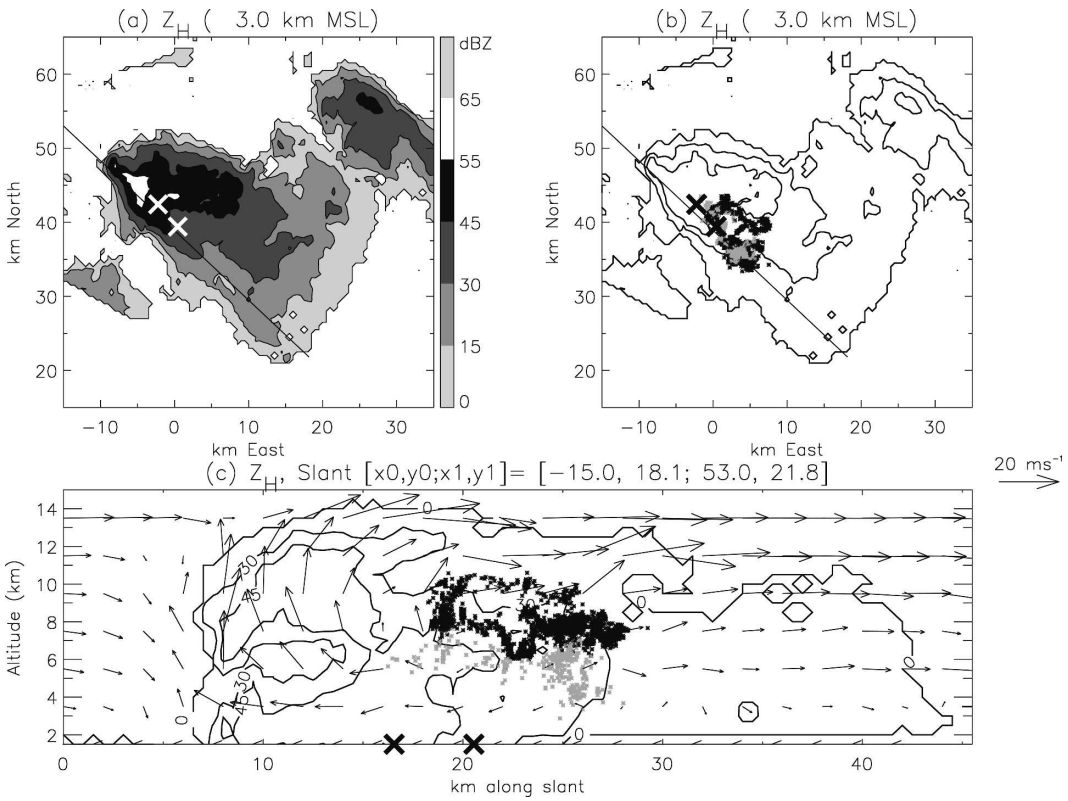

FIG. 15. Radar cross sections of radar reflectivity (Z_H) for volume scan beginning at 2239 UTC. (b), (c) LMA sources from five normal IC flashes are overlaid and color-coded by inferred ambient charge region as in Fig. 14. For reference, NLDN strike points corresponding to the two +CG flashes shown in Fig. 16 are indicated by ×'s; Z_H is (a) gray-shaded and (b), (c) contoured with intervals of 0, 30, and 45 dBZ. Doppler-derived flow field is also shown in (c).

vault and midlevel BWER (Fig. 12, right column). As discussed in Part I, the flow diverged around the updraft, particularly to the south, leading to a reflectivity maximum southeast of the main updraft. Again, the lightning density mirrored the reflectivity structure in the mid- to upper levels (cf. the top two panels of the right column of Fig. 12). A pronounced midlevel lightning "hole" was coincident with the midlevel BWER, with active lightning above and downwind (especially southeast) of the BWER. As with 2239 UTC, the TFR increased dramatically (to nearly 150 min^{-1}), and the storm began producing frequent +CG flashes.

Though much of the lightning within the echo vault above the updraft consisted of compact flashes lacking clear vertical charge structure, there were still many flashes indicating an inverted dipole structure here and in the upper levels farther downwind (Fig. 12, bottom right panel). In addition, relatively infrequent normal IC flashes continued to indicate the presence of lower negative charge just downwind of the precipitation core. The seven +CG flashes during the 2325 UTC volume scan struck ground in two clusters. Each cluster appeared to be associated with the separate diverging flows around the updraft, with one cluster of three +CG flashes along the northeast path, and the other cluster of four +CG flashes along the more dominant southeast path. The initial negative breakdown of all seven +CG flashes progressed upward from 6–7 km into a distinct midlevel maximum of LMA density (positive charge) just downwind of the hail shaft (Fig. 12, right column, bottom two panels). Following their return strokes, most of them tapped additional midlevel positive charge extending south and east, but rarely extended back westward into the more intense precipitation. Leading up to the peaks in hail echo volume and +CG flash rate at 2343–2351 UTC, the majority of +CG flashes continued to cluster (in both origin and strike location) on the downwind side of the hail shaft along these divergent flow paths, tapping positive charge at 6.5–10 km MSL. Figure 18 shows a particularly clear example.

By 2351 UTC, the BWER had filled in with large hydrometeors, and the lightning activity had wrapped around it, leading to a pronounced peak in LMA den-

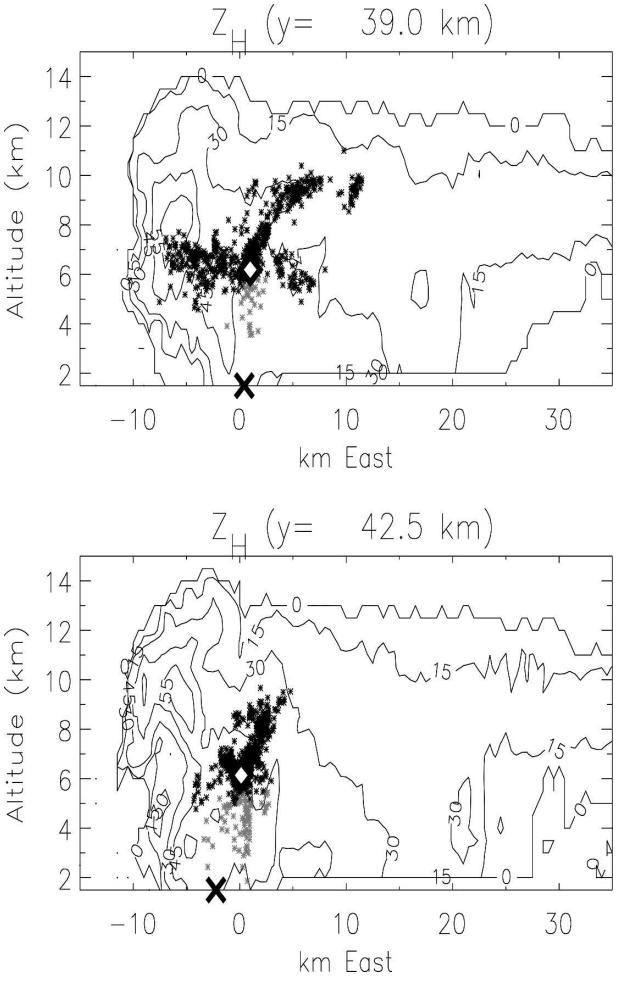

FIG. 16. Vertical cross sections of radar reflectivity (Z_H) for volume scan beginning at 2239 UTC with contour intervals of 0, 15, 30, 45, and 55 dBZ. LMA sources from the first two +CG flashes at (top) 2242:07 and (bottom) 2244:51 UTC are overlaid and color-coded by inferred ambient charge region as in Fig. 14. The filled diamond symbols aloft indicate the first LMA sources of each flash while the black X symbols along the ground indicate the NLDN strike points.

sity on the western side of the updraft (Fig. 13, left column, top two panels). Flashes in this western portion of the hail shaft generally indicated an inverted dipole with a deep (5–9 km MSL) positive charge region below a negative charge region (Fig. 13, bottom left panel). The two +CG flashes that struck south of the updraft tapped this deep positive charge region. The remainder of the +CG flashes also showed limited propagation into the positive charge in the hail shaft, but the majority of the breakdown continued to be through midlevel positive charge extending eastward from the downwind edge of the hail.

From 0000 to 0030 UTC, the storm continued to produce frequent inverted flashes in the upper levels (≈8–12 km MSL), though we did not attempt to diagnose the detailed charge structure from the LMA data. However, MacGorman et al. (2005) report on the charge structure inferred from an instrumented balloon flown through the storm during this time. Within the updraft, they found positive charge from 8–10 km, with alternating negative/positive/negative charge above, with the uppermost negative charge at 12–13 km MSL. Along the descent, they again found positive charge from 9.5–12 km with four additional regions of charge below, alternating in polarity with positive charge at 5.8–8 km and below 4 km. They posited that +CG flashes could involve any of the positive charge regions found in the downward sounding. The lightning mapping of the +CG flashes showed that the majority of them continued to cluster near and downwind of the precipitation core, and involved inferred negative charge at 5–7 km and positive charge at 7–9 km, which roughly corresponds to the midlevel charge structure inferred from the downward balloon sounding. However, a half dozen or so +CG flashes initiated to the south-southeast of the hail, with little discernible structure other than extensive low-level breakdown back westward into the hail core (e.g., Fig. 19). This extreme lower-level charge may correspond to the lowest positive charge region of the balloon sounding. Comparison of the lightning mapping with the balloon sounding is difficult, however, because the LMA-inferred charge structure varied greatly in the horizontal while the balloon measured only along its flight path.

During the radar volume scan at 0030 UTC, the +CG flash rate peaked and the +CG strikes clustered along a roughly north–south line 5–15 km east of the elongated hail shaft (Fig. 13, middle column). Exterior to the updraft and hail core, the lightning-mapped structure of the flashes was relatively consistent and revealed a basic inverted tripole charge structure. Keeping with the recurring theme of this storm, the initial inferred negative breakdown of most of the +CG flashes progressed upward into the eastern, downward-sloping positive charge of this inverted tripole. However, unlike during previous peaks in +CG flash rate, both the strike points and continued propagation of the +CG flashes during the 0030 UTC volume scan were markedly further downwind of the hail core. The one −CG flash during this time, however, initiated near the top of the hail core and descended through it (and presumably through positive charge). Figure 20 shows the lightning mapping of this −CG flash along with a representative +CG flash further downwind. There were a few other instances like this of −CG flashes initiating near the top of the hail shaft and propagating through it, while the +CG flashes clustered further downwind.

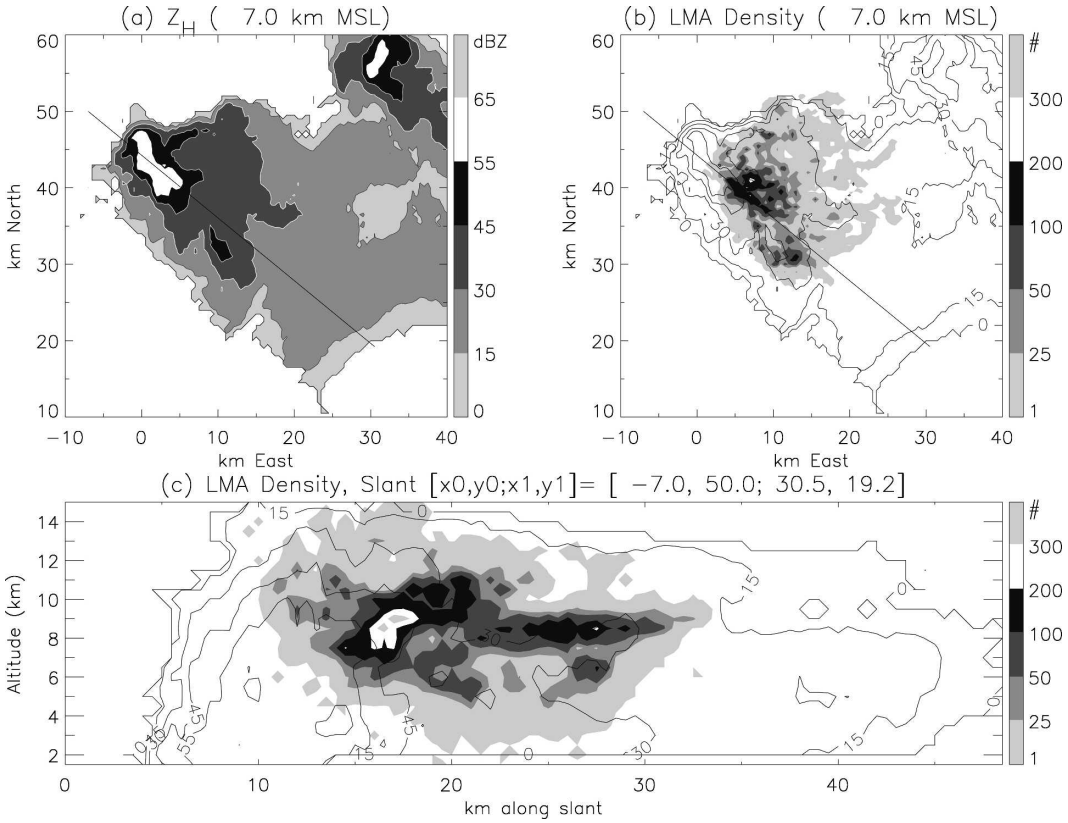

FIG. 17. Cross sections of (a) radar reflectivity (Z_H) for volume scan beginning at 2252 UTC and (b), (c) LMA density during the first 4 min of this volume scan. LMA density includes all sources within 5 km of each cross section. Contours of Z_H are gray-shaded in (a) and repeated in (b) and (c) with intervals of 0, 15, 30, 45, 55, and 65 dBZ.

Perhaps in these situations the magnitudes of the charge regions in the hail core were more similar to those of a normal tripole, particularly in terms of the lower positive charge, such that negative breakdown was able to propagate through the lower positive charge on to ground.

4) DECLINING PHASE (0036–0115 UTC)

As the updraft, graupel, and hail echo volumes steadily declined from 0036–0115 UTC (Fig. 5), the bulk of the lightning activity steadily descended (Fig. 6b). During the last volume scan of the observation period (0115 UTC), the +CG flash rate reached its absolute maximum, and all but four of the 23 +CG flashes from 0115 to 0120 UTC struck ground in a very tight cluster nearly coincident with the hail swath beneath a very dense concentration of LMA sources (Fig. 13, right column). The +CG flashes were so clustered that it is difficult to resolve the individual strike points or to discern the underlying storm structure in this figure. In contrast to earlier times, almost all of these +CG flashes tapped the inferred positive charge in the hail shaft (e.g., Fig. 21), though some also continued to tap into midlevel (6–8 km MSL) positive charge further east, downwind of the hail shaft. Of the two −CG flashes during this time, one struck in the hail shaft and one northeast of it.

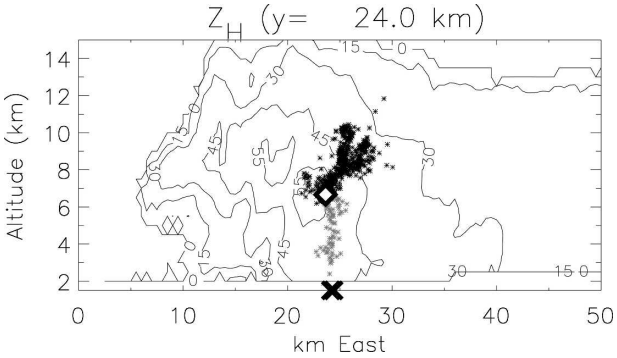

FIG. 18. Vertical cross section of radar reflectivity (Z_H) for volume scan beginning at 2331 UTC with intervals of 0, 15, 30, 45, and 55 dBZ. LMA sources from the +CG flash at 2334:38 UTC are overlaid and color-coded by inferred ambient charge region as in Fig. 14. The filled diamond symbol indicates the first source of the flash, and the black × symbol indicates the NLDN strike point.

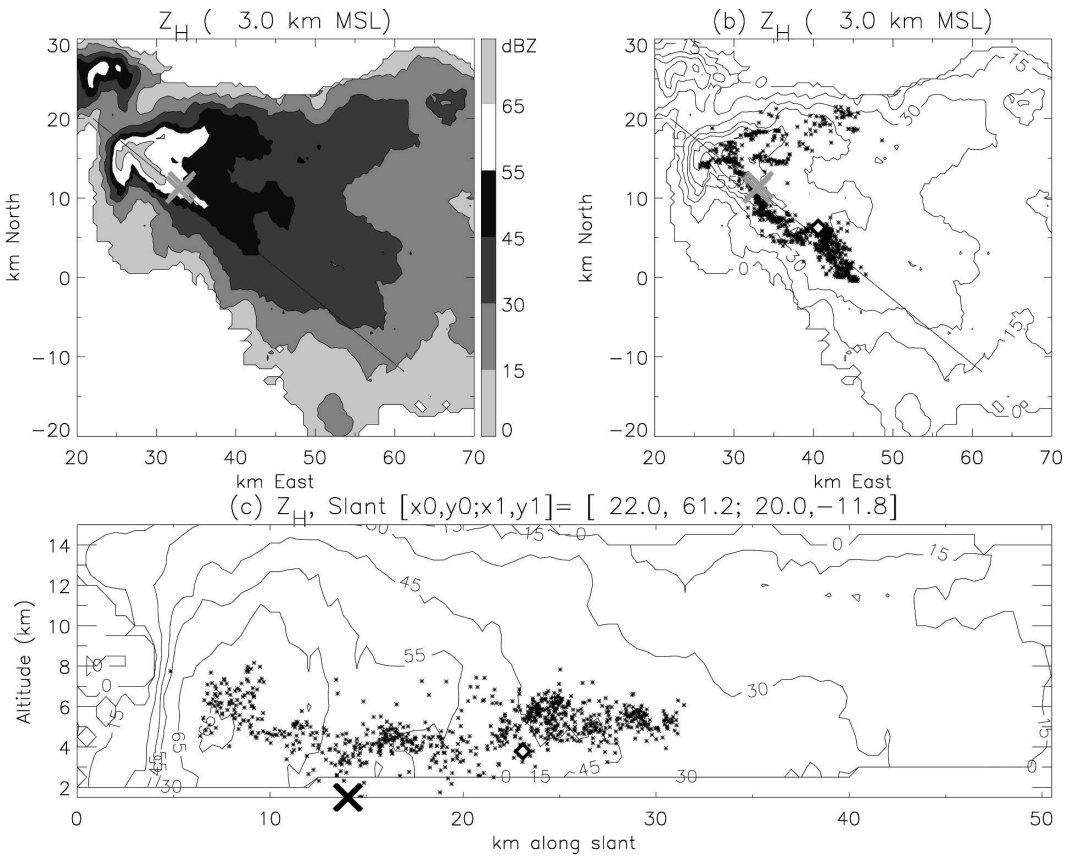

FIG. 19. Radar cross sections of radar reflectivity (Z_H) for volume scan beginning at 0010 UTC. (b), (c) LMA sources from the +CG flash at 0013:15 UTC are overlaid with no charge color-coding. Diamond symbols indicate the first source of the flash and × symbols indicate the NLDN strike point. Contours of Z_H are (a) gray-shaded and (b), (c) repeated with intervals of 0, 15, 30, 45, 55, and 65 dBZ.

Both initiated near 9 km MSL, atop the LMA density maximum (Fig. 13, right column, third and fourth panels).

4. Summary and discussion

The following points summarize the key observations of this study.

1) The LMA-inferred total flash rate (TFR) reached nearly 300 min^{-1}, with IC flashes accounting for 95%–100% of the total lightning activity during any given minute. Nearly 90% of the CG flashes delivered positive charge to ground, with a peak +CG flash rate of nearly 5 min^{-1}.
2) The TFR was well correlated temporally with volumes of updraft ($w > 10$ m s^{-1}) and inferred graupel echo. The latter correlation highlights the importance of charge-separating collisions within the mixed-phase region that are crucial to thunderstorm electrification. TFR was decidedly less correlated with hail echo volume, and the lightning sometimes avoided the >55 dBZ hail shaft, suggesting that hail plays less of a role in charge separation.
3) As shown in the schematic of Fig. 22, the LMA-inferred charge structure of this storm varied greatly in the horizontal and with time. The first 20 min (2130–2150 UTC) of lightning activity in this storm indicated a charge structure consisting solely of a negative charge region at an altitude of 7–8 km ($-10° < T < -15°$C) and a positive charge region at 4–5 km ($T \approx 0°$C), with no indication of an upper positive charge. Then, shortly after a strong surge in updraft, the storm rapidly developed upper-level (>8 km MSL) charge regions that dominated the ensuing lightning activity. For a brief period of time (≈2150–2230 UTC) after this surge in updraft and lightning, the storm exhibited a distinct vertically stratified charge structure that consisted of five charge regions, alternating in polarity, with positive nearest the ground. Over the remainder of the observation period (2230–0115 UTC), the lightning

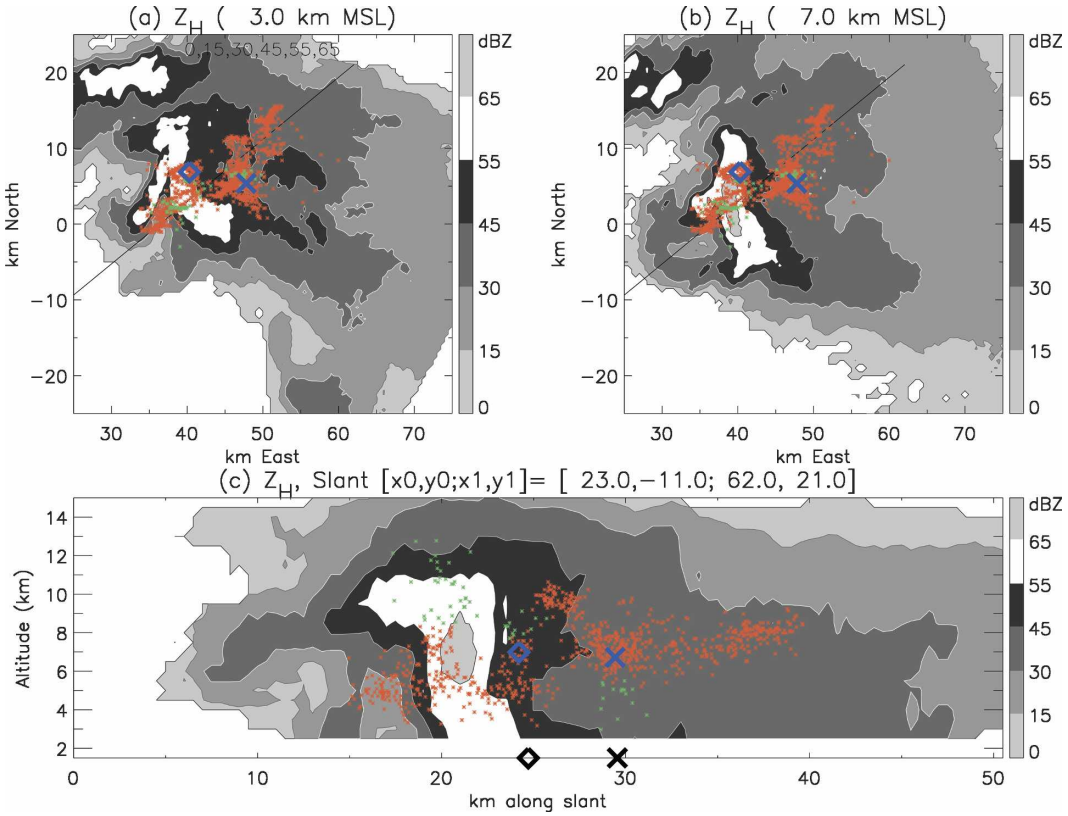

FIG. 20. Radar cross sections for volume scan beginning at 0030 UTC. LMA sources from a −CG flash and a +CG flash are overlaid and color-coded by inferred ambient charge region, with red for positive and green for negative. In the horizontal cross sections, the blue ×'s and diamonds indicate the +CG and −CG strike points, respectively. In the vertical cross section, the blue × and diamond aloft indicate mean origin location of the CG flashes while the black × and diamond indicate their NLDN strike points.

was very intense and the charge structure was less obvious. However, the storm consistently produced a dominant upper level (≈8–12 km MSL) inverted dipole charge structure near the updraft. This basic inverted dipole structure also extended downwind but sloped downward with additional negative charge beneath it. The term inverted tripole is thus a reasonably accurate description of this charge structure, but a simple vertical description would be a gross oversimplification.

4) The +CG flashes of this storm all originated from 5–9-km altitude and generally clustered on the downwind side of the main precipitation/hail core. The initial breakdown of the vast majority of the +CG flashes progressed upward from the lower negative charge into the midlevel positive charge of the inverted tripole described above. The +CGs tapped positive charge within the hail shaft and (more frequently) from the midlevel (6–8 km MSL) positive charge region extending farther downwind.
5) Finally, lightning holes were often coincident with bounded weak echo regions (BWERs), with active lightning in the strong lofted radar echo above the BWER. In their LMA observations of tornadic storms in Oklahoma, Krehbiel et al. (2000a) noted similar lightning holes in otherwise volume-filling lightning activity. Hence, there is little doubt that,

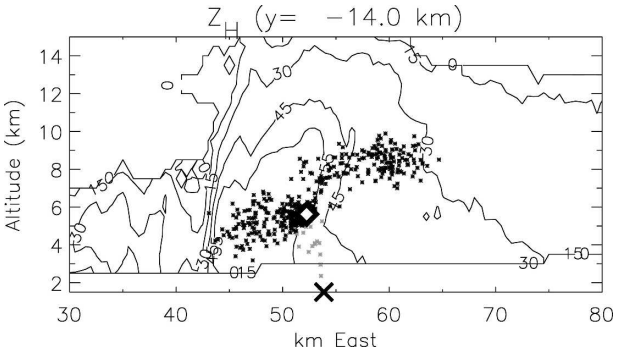

FIG. 21. As in Fig. 18, but for the volume scan beginning at 0015 UTC with the +CG flash at 0117:21 UTC.

like BWERs, such lightning holes are indicators of strong, broad updrafts and hence may have some value as an indicator of severe weather.

How did this storm form the deep, persistent midlevel region of positive charge tapped by its +CG flashes? As suggested by Williams (2001) in his discussion of +CG-dominated storms, one possible explanation is that the strong, broad updraft suffered less entrainment, which allowed supercooled liquid water (SLW) contents to reach near adiabatic values in the mixed-phase region. According to laboratory results of the noninductive ice collisional charging (NIC) mechanism (e.g., Takahashi 1978; Saunders and Peck 1998), this would lead to positive charging of graupel and hail over a greater (i.e., colder) range of temperatures, thus shrinking (or removing altogether) the region of negative graupel/hail charging within the core of the updraft. These conditions also provide a prime environment for rapid hail growth (if the conditions outlined in Part I are also met). Hence, in this scenario, the coincident hail and +CG flash production of this storm are both the products of strong broad updraft in a SLW-rich environment. Carey et al. (2003a) proposed a similar explanation for the +CG dominance of the 1998 tornadic storm in Spencer, South Dakota (though there was less evidence of associated hail formation in their study). The results of Lang and Rutledge (2002) offer further support. Their study included eleven storms that spanned a wide range of severity. In general, they found that −CG flash production decreased with increased updraft and hail production. The two storms of their study (one of which was the 29 June 2000 storm) that had the strongest, broadest updrafts and greatest hail production, also produced predominantly +CG flashes. Severe hailstorms are not always dominated by +CG flashes, so there is still something unique about the environment of the STEPS region that the observations have yet to reveal.

The results of this study show that much as lower positive charge appears to be a requirement for −CG flashes in normal tripole thunderstorms, the presence of a lower negative charge region appeared to be a requirement for the +CG flashes of this storm. This lower negative charge was revealed not only by +CG flashes but also by IC flashes. The presence of a lower negative charge did not guarantee +CG flashes in this storm, but as far as could be determined from the LMA data, +CG flashes did not occur without it. Assuming (as described above) the NIC mechanism led to predominantly positive charging of graupel and hail and thus to the formation of the deep positive charge region of this storm, how then did the lower negative charge form, and how was it maintained? Numerical simulations of this storm by Kuhlman (2004) offer some intriguing clues. In these simulations, collisions in the SLW-rich core of the updraft granted positive charge to graupel and hail, resulting in the observed deep positive charge region and inverted dipole charge structure. Collisions on the (relatively SLW deficient) periphery of the updraft led to negative charging of graupel, leading to the lower negative charge farther downwind.

These simulation results and reexamination of the observations of this and other storms during STEPS (see, e.g., Wiens 2005) led to the following ideas about what led to the charge structure during the severe +CG-producing phase of this storm. The central ideas are that the sign of the charging was dependent on the location of the collisions relative to the updraft, and that the particles involved in the collisions were segregated by the wind flow based on their sizes and associated fall speeds. These ideas are illustrated in the right side of Fig. 22. As in the simulations, the positive charging of hail and graupel extended to colder temperatures within the SLW-rich core of the broad, strong updraft. This led to an inverted dipole charge structure near the updraft, with ice crystals carrying the negative charge and larger graupel and hail carrying the positive charge. In the SLW-deficient periphery of the updraft, collisions more often imparted negative charge to graupel and positive charge to ice crystals. The vertical wind shear was strong in this storm, which forced the precipitation forming in the updraft to fall out downwind, thus offsetting the precipitation core from the updraft core. We speculate that the hail growing in the strong updraft fell out directly, carrying the lower positive charge with it. The negatively charged ice crystals that collided with hail in the updraft core were lofted much higher and were then advected much farther downwind, leading to the horizontally extensive upper negative charge region. The midlevel positive and lower negative charge regions downwind of the updraft core may have formed because of collisions in the SLW-deficient periphery of the updraft, which more often imparted negative charge to graupel and positive charge to ice crystals. The negatively charged graupel then descended to form the lower negative charge region adjacent to and downwind of the hail. The resulting inverted tripole charge structure downwind of the hail core supported the frequent +CG flashes (Fig. 22).

This explanation is certainly oversimplified. The overall charge structure was likely a superposition of the charging processes both within and on the periphery of the updraft. For example, advection of the positively charged particles in the core of the updraft may have also contributed to the midlevel positive charge

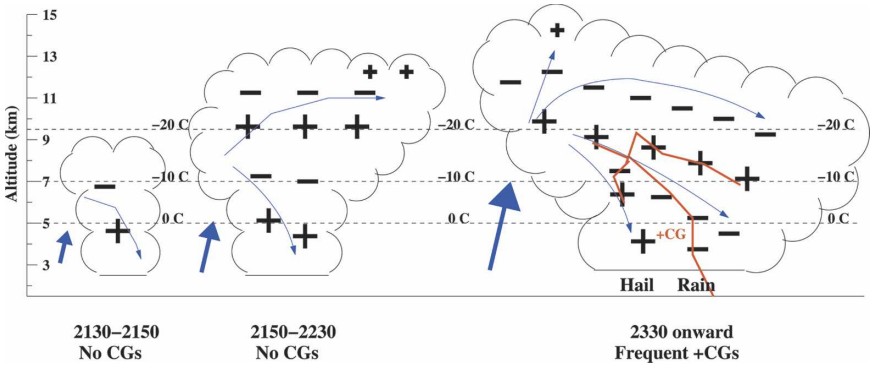

FIG. 22. Schematic idealization of the evolution of the 29 Jun supercell. Thick blue arrows show main updraft, and thin blue arrows show airflow. Plus and minus symbols show the gross LMA-inferred charge structure. The red disjointed lines show the idealized breakdown path of a representative +CG discharge.

downwind. Furthermore, as suggested by Stolzenburg et al. (1998c), the NIC mechanism may not have been the only electrification process operating.

Acknowledgments. We thank Paul Krehbiel, William Rison, Ron Thomas, Tim Hamlin, and Jeremiah Harlin of New Mexico Tech for the LMA data, software, and expertise. Thanks to Larry Carey of Texas A&M and Jay Miller of NCAR for very valuable discussion and assistance with the radar data. A very thorough anonymous reviewer led to significant improvement of this paper. This research was funded by SOARS, an American Meteorological Society Graduate Fellowship, and NSF Grant ATM-9912051. The CSU–CHILL radar facility is sponsored by the NSF Cooperative Agreement ATM-0118021 and Colorado State University. The S-Pol radar, operated by NCAR, is funded by the NSF.

REFERENCES

Berdeklis, P., and R. List, 2001: The ice crystal–graupel charging mechanism of thunderstorm electrification. *J. Atmos. Sci.,* **58,** 2751–2770.

Brook, M., M. Nakano, P. Krehbiel, and T. Takeuti, 1982: The electrical structure of the Hokuriku winter thunderstorms. *J. Geophys. Res.,* **87,** 1207–1215.

Carey, L. D., and S. A. Rutledge, 1996: A multiparameter radar case study of the microphysical and kinematic evolution of a lightning producing storm. *Meteor. Atmos. Phys.,* **59,** 33–64.

——, and ——, 1998: Electrical and multiparameter radar observations of a severe hailstorm. *J. Geophys. Res.,* **103,** 13 979–14 000.

——, W. A. Petersen, and S. A. Rutledge, 2003a: Evolution of cloud-to-ground lightning and storm structure in the Spencer, South Dakota, tornadic supercell of 30 May 1998. *Mon. Wea. Rev.,* **131,** 1811–1831.

——, S. A. Rutledge, and W. A. Petersen, 2003b: The relationship between severe storm reports and cloud-to-ground lightning polarity in the contiguous United States from 1989 to 1998. *Mon. Wea. Rev.,* **131,** 1211–1228.

Coleman, L. M., T. C. Marshall, M. Stolzenburg, T. Hamlin, P. R. Krehbiel, W. Rison, and R. J. Thomas, 2003: Effects of charge and electrostatic potential on lightning propagation. *J. Geophys. Res.,* **108,** 4298, doi:10.1029/2002JD002718.

Cummins, K. L., M. J. Murphy, E. A. Bardo, W. L. Hiscox, R. B. Pyle, and A. E. Pifer, 1998: A combined TOA/MDF technology upgrade of the U.S. National Lightning Detection Network. *J. Geophys. Res.,* **103,** 9035–9044.

Curran, E. B., and W. D. Rust, 1992: Positive ground flashes produced by low-precipitation thunderstorms in Oklahoma on 26 April 1984. *Mon. Wea. Rev.,* **120,** 544–553.

Hamlin, T., 2004: The New Mexico Tech Lightning Mapping Array. Ph.D. dissertation, New Mexico Institute of Mining and Technology, 164 pp.

——, J. D. Harlin, P. R. Krehbiel, W. Rison, and R. J. Thomas, 2001: Lightning as a detector of convective surges in thunderstorms. *Eos, Trans. Amer. Geophys. Union,* **82** (Suppl.), Abstract AE12A-86.

Jacobson, E. A., and E. P. Krider, 1976: Electrostatic field changes produced by Florida lightning. *J. Atmos. Sci.,* **33,** 103–117.

Kasemir, H. W., 1960: A contribution to the electrostatic theory of lightning discharge. *J. Geophys. Res.,* **65,** 1873–1878.

Krehbiel, P. R., M. Brook, and R. A. McCrory, 1979: An analysis of the charge structure of lightning discharges to ground. *J. Geophys. Res.,* **84,** 2432–2456.

——, R. J. Thomas, W. Rison, T. Hamlin, J. Harlin, and M. Davis, 2000a: GPS-based mapping system reveals lightning inside storms. *Eos, Trans. Amer. Geophys. Union,* **81,** 21–25.

——, ——, ——, ——, ——, M. Stanley, J. Lombardo, and D. Shown, 2000b: Inverted polarity lightning in STEPS. *Eos, Trans. Amer. Geophys. Union,* **81** (Suppl.), Abstract A62D-06.

Kuhlman, K. M., 2004: Numerical simulations of the 29 June 2000 STEPS tornadic supercell: Microphysics, electrification, and lightning. Master's thesis, Dept. of Meteorology, University of Oklahoma, 72 pp.

Lang, T. J., and S. A. Rutledge, 2002: Relationships between convective storm kinematics, precipitation, and lightning. *Mon. Wea. Rev.,* **130,** 2492–2506.

——, and Coauthors, 2004a: The Severe Thunderstorm Electrification and Precipitation Study (STEPS). *Bull. Amer. Meteor. Soc.,* **85**, 1107–1125.

——, S. A. Rutledge, and K. C. Wiens, 2004b: Origins of positive cloud-to-ground lightning flashes in the stratiform region of a mesoscale convective system. *Geophys. Res. Lett.,* **31,** L10105, doi:10.1029/2004GL019823.

Larson, H. R., and E. J. Stansbury, 1974: Association of lightning flashes with precipitation cores extending to height 7 km. *J. Atmos. Terr. Phys.,* **36,** 1547–1553.

MacGorman, D. R., and D. W. Burgess, 1994: Positive cloud-to-ground lightning in tornadic storms and hailstorms. *Mon. Wea. Rev.,* **122,** 1671–1697.

——, ——, V. Mazur, W. D. Rust, W. L. Taylor, and B. C. Johnson, 1989: Lightning rates relative to tornadic storm evolution on 22 May 1981. *J. Atmos. Sci.,* **46,** 221–250.

——, W. D. Rust, P. Krehbiel, W. Rison, E. Bruning, and K. Wiens, 2005: The electrical structure of two supercell storms during STEPS. *Mon. Wea. Rev.,* **133,** 2583–2607.

Mansell, E. R., 2000: Electrification and lightning in simulated supercell and non-supercell thunderstorms. Ph.D. dissertation, University of Oklahoma, 211 pp.

——, D. R. MacGorman, C. L. Ziegler, and J. M. Straka, 2002: Simulated three-dimensional branched lightning in a numerical thunderstorm model. *J. Geophys. Res.,* **107,** 4075, doi:10.1029/2000JD000244.

Marshall, T. C., and M. Stolzenburg, 2002: Electrical energy constraints on lightning. *J. Geophys. Res.,* **107,** 4052, doi:10.1029/2000JD000024.

Mazur, V., and L. H. Ruhnke, 1993: Common physical processes in natural and artificially triggered lightning. *J. Geophys. Res.,* **98,** 12 913–12 930.

Orville, R. E., and G. R. Huffines, 2001: Cloud-to-ground lightning in the United States: NLDN results in the first decade, 1989–98. *Mon. Wea. Rev.,* **129,** 1179–1193.

Proctor, D. E., 1991: Regions where lightning flashes began. *J. Geophys. Res.,* **96,** 5099–5112.

Rhodes, C. T., X. M. Shao, P. R. Krehbiel, R. J. Thomas, and C. O. Hayenga, 1994: Observations of lightning phenomena using radio interferometry. *J. Geophys. Res.,* **99,** 13 059–13 082.

Rison, W., R. J. Thomas, P. R. Krehbiel, T. Hamlin, and J. Harlin, 1999: A GPS-based three-dimensional lightning mapping system: Initial observations in central New Mexico. *Geophys. Res. Lett.,* **26,** 3573–3576.

Rust, W. D., and D. R. MacGorman, 2002: Possibly inverted-polarity electrical structures in thunderstorms during STEPS. *Geophys. Res. Lett.,* **29,** 1571, doi:10.1029/2001GL014303.

——, and Coauthors, 2005: Inverted-polarity electrical structures in thunderstorms in the Severe Thunderstorm Electrification and Precipitation Study (STEPS). *Atmos. Res.,* **76,** 247–271.

Saunders, C. P. R., and I. M. Brook, 1992: The effects of high liquid water contents on thunderstorm charging. *J. Geophys. Res.,* **97,** 14 671–14 676.

——, and S. L. Peck, 1998: Laboratory studies of the influence of the rime accretion rate on charge transfer during graupel/crystal collisions. *J. Geophys. Res.,* **103,** 13 949–13 956.

Shao, X. M., and P. R. Krehbiel, 1996: The spatial and temporal development of intracloud lightning. *J. Geophys. Res.,* **101,** 26 641–26 668.

Stolzenburg, M., 1994: Observations of high ground flash densities of positive lightning in summertime thunderstorms. *Mon. Wea. Rev.,* **122,** 1740–1750.

——, W. D. Rust, and T. C. Marshall, 1998a: Electrical structure in thunderstorm convective regions. 2. Isolated storms. *J. Geophys. Res.,* **103,** 14 079–14 096.

——, ——, B. F. Stull, and T. C. Marshall, 1998b: Electrical structure in thunderstorm convective regions. 1. Mesoscale convective systems. *J. Geophys. Res.,* **103,** 14 059–14 078.

——, ——, and T. C. Marshall, 1998c: Electrical structure in thunderstorm convective regions. 3. Synthesis. *J. Geophys. Res.,* **103,** 14 097–14 108.

Takahashi, T., 1978: Riming electrification as a charge generation mechanism in thunderstorms. *J. Atmos. Sci.,* **35,** 1536–1548.

Tessendorf, S. A., L. J. Miller, K. C. Wiens, and S. A. Rutledge, 2005: The 29 June 2000 supercell observed during STEPS. Part I: Kinematics and microphysics. *J. Atmos. Sci.,* **62,** 4127–4150.

Thomas, R., P. Krehbiel, W. Rison, J. Harlin, T. Hamlin, and N. Campbell, 2003: The LMA flash algorithm. *Proc. 12th Int. Conf. on Atmospheric Electricity,* Versailles, France, ICAE, 655–656.

——, P. R. Krehbiel, W. Rison, S. J. Hunyady, W. P. Winn, T. Hamlin, and J. Harlin, 2004: Accuracy of the Lightning Mapping Array. *J. Geophys. Res.,* **109,** D14207, doi:10.1029/2004JD004549.

Wiens, K. C., 2005: Kinematic, microphysical, and electrical structure and evolution of thunderstorms during the Severe Thunderstorm Electrification and Precipitation Study (STEPS). Ph.D. dissertation, Colorado State University, 295 pp.

Williams, E. R., 1989: The tripole structure of thunderstorms. *J. Geophys. Res.,* **94,** 13 151–13 167.

——, 2001: The electrification of severe storms. *Severe Convective Storms, Meteor. Monogr.,* No. 50, Amer. Meteor. Soc., 527–561.

——, C. M. Cooke, and K. A. Wright, 1985: Electrical discharge propagation in and around space charge clouds. *J. Geophys. Res.,* **90,** 6059–6070.

——, and Coauthors, 1999: The behavior of total lightning activity in severe Florida thunderstorms. *Atmos. Res.,* **51,** 245–264.

Zajac, B. A., and S. A. Rutledge, 2001: Cloud-to-ground lightning activity in the contiguous United States from 1995 to 1999. *Mon. Wea. Rev.,* **129,** 999–1019.

Zhang, Y., P. R. Krehbiel, T. Hamlin, J. Harlin, R. Thomas, and W. Rison, 2001: Electrical charge structure and cloud-to-ground lightning in thunderstorms during STEPS. *Eos, Trans. Amer. Geophys. Union,* **82** (Suppl.), Abstract AE12A-0079.